Measuring wave transformation in a tidal inlet using Wave Resolving Drifters

Additional Master Thesis

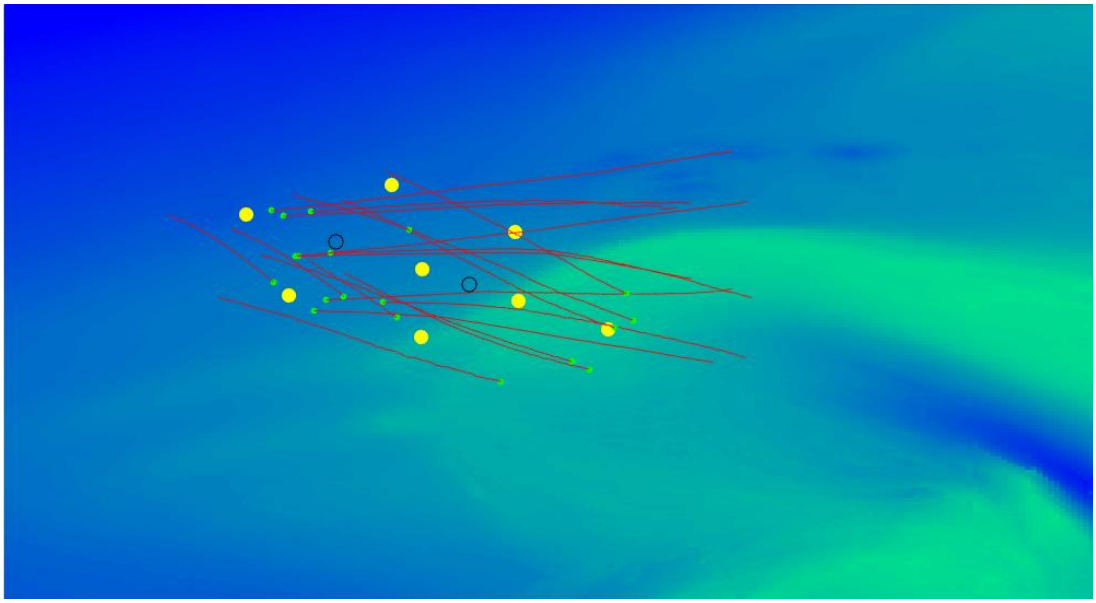

A.B. van Langevelde

November 24, 2017

TU Delft Delft University of Technology

PREFACE

This is the report on the research that is done as an Additional Master Thesis for the track Hydraulic Engineering of the master Civil Engineering at the TU Delft (CIE5050-09).

This research project is a part of the SEAWAD research project, a research project on sand nourishment in the Wadden Sea coastal region. Multiple research institutions, governmental organisations and companies take part in this research. This report handles a part of the research on measurements of the wave conditions in favour of the research on intra wave sediment transport.

For the realization of this report I'm thankful to people. First of all thanks to Floris and Marion for their participation in thinking, their comments and their overall support. Thanks to Stuart and Thomas for the provision of some required information. Thanks to Max for the support on the WaveDroid: the help in processing and the time made for answering question. Finally thanks to all who have been supporting me, either on the content or in the process.

Bart van Langevelde
Delft, November 2017

ABSTRACT

In the coastal defence of the Netherlands, sand nourishment is a common practice. Part of the Dutch coastal system, the Wadden Sea coast, is a very complicated coastal system in terms of hydrodynamics and morphodynamics. Many different processes are playing a role in the coastal dynamics in the Wadden Sea area. The execution of a mega nourishment in this area is intended. To make this possible, the dynamics of the system must be understood better than they are today.

Part of the coastal dynamic system is the intrawave sediment transport. To improve understanding of this phenomenon, research is done on the wave conditions in a tidal inlet of the Wadden Sea. In the accompanying field campaign use is made of unanchored WaveDroids, used as wave resolving drifter. This is the first time unanchored use of WaveDroids is carried out. The use of a moving measurement device gives rise to differences in measurement results compared to the known approach with fixed measurement devices.

This research shows the difficulties that must be overcome to process raw measurement data in such a way that the data becomes suitable for analysis and interpretation. The data is filtered on frequency and on wave height to give a useful representation of the wave field. The processed data is assessed on the energy density spectrum, the wave height distributions and the time series of wave heights and surface elevation. Subsequently, in the interpretation of the selected data, insight is given in the measured wave field.

From this research is concluded that the use of WRD's is suitable to measure the vertical component of wave displacement. The effect of a Doppler shift, originating from the use of different frames of reference, is not significant is common sea states. The measurement of the horizontal component of wave displacement requires more research on correcting processing steps.

TABLE OF CONTENT

PREFACE i
ABSTRACT iii
TABLE OF CONTENT v
1. Introduction 1
1.1. SEAWAD 1
1.2. Research using Wave Resolving Drifters 2
2. Literature 5
2.1. Frames of reference 5
2.2. Wave – current interaction 6
2.3. Wave height distribution 6
3. Methodology 9
3.1. Description of the measurement campaign 9
3.1.1. Local environment 9
3.1.2. The Drifters in SEAWAD Field Campaign 10
3.2. Wave resolving drifters 13
3.3. Frame of reference 14
4. Results 15
4.1. Measurement results 15
4.1.1. Preparatory raw data processing 16
4.1.1.1. Data conversion 16
4.1.1.2. Frequency filter 16
4.1.1.3. Time step correction 17
4.1.1.4. Magnetic correction 18
4.1.2. Correcting data processing 18
4.1.2.1. Low frequency energy 19
4.1.2.2. Erroneous large waves 20
4.1.2.3. Data selection 23
4.2. Data analysis results 24
4.2.1. Wave-by-wave analysis 25
4.2.2. Spectral analysis 28
4.2.3. Comparing frames of reference 30
4.2.3.1. Theoretical Doppler shift 30

4.2.3.2. Measurements of different frames of reference 31
5. Conclusions 35
5.1. Conclusions 35
5.2. Discussions 35
5.3. Recommendations 36
References 37
Figures 39
Tables 40
Appendix I
A. Data management I
B. Variances V
C. Remaining data for analysis VII
D. All results wave-by-wave analysis XI
E. All results spectral analysis XV

1. Introduction

Sea level rise is a threat to the subsiding, already low laying Dutch areas by eroding the coastal system (Hinkel, et al., 2013). This erosion is counterbalanced by sand nourishments at the coast. The Wadden Sea basins import sediment from the coasts of Holland and the Wadden Sea barrier islands to adjust to the rising sea level. Besides that, the Wadden Sea basins are still importing sediment to adjust to the closure of the Zuider Sea and the Lauwers Sea (Elias, et al., 2012). Due to the acceleration of both absolute and relative sea level rise the magnitude of future sand nourishments will increase, making coastal maintenance even more costly. A mega nourishment, a new phenomenon in coastal maintenance, is the nourishment of a large amount of sand at one location. The sand then is transported by natural phenomena to its intended location on the coastal defense. Application of a mega nourishments increases the cost effectiveness of the nourishments.

The application of mega nourishments is in its infancy. Existing experience with a mega nourishment was gained at the straight coast of Holland, with the Sand Motor (Stive, et al., 2013). Knowledge gained at that location cannot be translated directly to a mega nourishment in an area like the Wadden Sea, because of its complicated hydrodynamics and morphodynamics. Furthermore, the Wadden Sea has a large ecological value and has a protected status. As a consequence, each possible interference with the natural system must be approached with much cautiousness.

1.1. SEAWAD

SEAWAD (SEdiment supply At the WAdden Sea ebb-tidal Delta) is a research project that investigates the possibilities of a mega nourishment for the Wadden Sea by nourishing the ebb tidal delta. The Wadden Sea area is a very complex system in terms of hydrodynamics and morphodynamics. It contains basins, inlets, shallows, wave action, tidal currents and wave-current interaction. SEAWAD aims to gain knowledge on complex systems like these to be able to predict the consequences of a nourishment. One of the knowledge gaps that is identified for SEAWAD is on the effect of intrawave sediment transport processes on large-scale sediment transport.

The common way of predicting the consequences of an engineering interference on a natural system is the approach by computer models. Two of the more advanced types of morphological models can be distinguished by scale. These types of models are the short-term quasi-deterministic model and long-term schematized model. The short-term model can be calibrated to high accuracy but is very costly in terms of calculation time. The long-term model gives a good representation of the influence of large bathymetric features but lacks the influence of individual waves due to wave averaging. The wave-averaging in long-term models is usually resulting in parametrization based on local characteristics. These parameterisations are obtained in absence of tidal flows (Ruessing, et al., 2012). It can be concluded that both models do not represent the morphodynamics well in a large highly dynamic environment like an inlet.

For long term engineering, that is on a scale of decades (which is shorter than the long term that long-term models are built for), a need exists for another type of model. Such a type of model, called a mid-term model, has of the accuracy of the short-term models as much as possible and has the ability to range over large time scales of the long term models. This model is not well developed yet. Experience with the more suitable mid-term is scarce and the predictive ability of

this type of model turns out to be not sufficient (Oost, et al., 2014) (Elias, et al., 2012). SEAWAD aims for the realization of a mid-term scale model for this specific case. In the context of realizing that model extensive measurements are executed in and around the inlet between Ameland and Terschelling.

One of the sections of the SEAWAD research project is the *Drifters in SEAWAD field campaign*. This field campaign is part of the section that researches intra-wave sediment transport. The field campaign consists of the deployment of current drifters and wave resolving drifters in a tidal inlet of the Wadden Sea. More detailed information on the field campaign is given in section 3.1.

1.2. Research using Wave Resolving Drifters

This research is on the application of wave resolving drifters (WRD's). WRD's are drifters that follow both the surface elevation and the currents, that is measuring in a Lagrangian frame of reference. (Section 3.2 elaborates more on WRD's.) It is known that WRD's can be used to measure waves. It is shown that results from WRD's, measuring with an accelerometer-tilt-compass sensor, show good comparison with the results from GPS based buoys (Herbers, et al., 2012). The conventional way of doing wave measurements is to use measurement devices that are fixed in its location, that is measuring in a Eulerian frame of reference. Whether the results from these WRD's are comparable with the results from fixed measurement devices is unanswered.

This research focuses on the usefulness of measuring with WRD's with respect to measuring with fixed devices. This research is executed in the larger research framework of understanding the hydrodynamics and morphodynamics in different conditions in the tidal basins of the Wadden Sea. This research is aimed at understanding the data that result from measurements by a WRD, the errors that occur in the data and ways of processing the data to make the data more suitable for further analysis.

In the end this research is aimed at developing a way to convert the results from the WRD's into a realistic and useful wave signal, containing information on the wave direction and wave height. This research aims to provide an answer to the following question:

> *What do wave resolving drifter data really represent and what post-processing of wave resolving drifter data is required to obtain a reliable representation of the wave conditions?*

The research question is divided into the following sub questions:

- What theoretical background is available on coastal dynamics in tidal inlets?
- What is the theoretical background on differences between an Eulerian and a Lagrangian framework and what is the influence of this on the measurement data?
- What steps of post-processing are needed to improve the data till the accuracy of the representation of a wave field is at an acceptable level?
- What insights on the wave conditions in a tidal inlet during a tidal wave, can be gained from the WRD measurement results?

This report treats the following subjects. The theoretical background on this subject is elaborated on in Chapter 3. This chapter handles the application of the Lagrangian frame of reference and relevant wave characteristics. More information on the measurement campaign and the measurement method is given in Chapter 3. Chapter 4 describes the development from raw data to data analysis step by step. First it elaborates on the steps taken to turn the raw data into more understandable quantities (section 4.1.1). Then it elaborates on each step taken to eliminate observed errors and to improve the quality of the data set (section 4.1.2). Finally, the chapter takes a brief analysis and interpretation of the data (section 4.2). In the last chapter the conclusions are drawn and discussed and recommendations for further work on this subject are given.

2. Literature

In this section existing knowledge on the subject of research is shown. It treats different subjects that are all relevant to the research. Section 2.1 elaborates on the difference between methods of observation in different frames of reference. Section 2.2 explains about the interaction between the forces that are present in waves and currents. This interaction can be expected in the research area. Finally, section 2.3 elaborates on wave height distribution that can be expected in the research area. In the remainder of this report the relevance of the literature becomes clearer.

2.1. Frames of reference

The motion of matter can be considered in two different reference frames: a Eulerian and a Lagrangian reference frame. A Eulerian reference frame has a point of view (hence an origin of axis) that is fixed in space. A Lagrangian reference frame has a point of view that is moving with the water particles. A WRD is moving in space, along with the water. In the context of a measurement campaign it is impossible to use a purely Lagrangian reference frame. A purely Lagrangian reference frame measures motion of water on the scale of a water particle and a WRD cannot measure water motion on the scale of a water particle because of its size and inertia. Therefore, when in the remainder of this report the term Lagrangian reference frame is mentioned it concerns a reference frame that is moving with the current and not with the water particles.

Measurements in different frames of reference observe waves in a slightly different way. The difference between the two wave signals is explained by the Doppler effect. A wave that is measured in a Eulerian reference frame shows the water level development in time on a fixed point in space. A wave that is measured in a Lagrangian reference frame shows the water level development in space and in time. Note that both are correct representations of the truth.

The observer in a moving frame of reference experiences a different particle velocity, a different wave speed and a different wave shape than an observer in a fixed frame of reference. The observer at a fixed point observes waves with a frequency ω; the absolute frequency. The observer moving with the current observes the same waves with the relative frequency σ. The absolute and relative frequency are related to each other:

Equation 1: $$\omega = \sigma + kU_n$$

In this equation k represents the wave number in rad/s and U_n represents the current velocity in the direction of wave propagation (Peregrine & Jonsson, 1983). The product of k and U_n is also known as the Doppler-shift. For data measured in a Eulerian reference frame this shift means that the wave signal is influenced by the current velocity. To be able to compare the measurement results from the WRD with other measurements or with existing knowledge on the subject (usually approaching the subject from a Eulerian point of view), it is useful to transform the data from the WRD to a Eulerian frame of reference.

2.2. Wave – current interaction

This research considers the wave measurements in the entrance channel of a tidal inlet. In such an inlet strong currents occur due to tidal current. Furthermore, because it is a nearshore environment, waves can play a significant role in the particle motion. Both the waves and the current can come from different directions. Each possible difference in the direction angle of the waves and the current, leads to a different interaction of waves and currents.

From laboratory modelling, it followed that an opposing current slows down a wave (Lai, et al., 1989). This delay imposes a compression in the length of the wave. This is comparable to the Doppler effect with the wave forcing acting as a transmitter of the wave signal and the current as a receiver. With the application of a Doppler-shift the wave signal from a Eulerian point of view, without the influence of a current, can be obtained. (Note that the relations between the forces and the waves are in practice more complicated than with a theoretical Doppler-relation. For instance, in the processes of wave forcing and wave current interactions, much energy dissipated. Furthermore, the theoretical relation does not account for the 2-dimensional character of a wave field.)

Another laboratory research, modelling an ebb situation has led to the insight that a current that opposes the waves, has an effect on the wave period and the wave shape (Briggs, et al., 1996). An oppposing current causes a amplification of the wave height, inducing growing wave steepness. This amplification is larger for a stronger current and for shorter wave periods. The opposing current furthermore adds energy to the frequencies of the wave spectra, that are above the frequency of the incoming waves. Multiplications of the amount of energy with a factor of 10 are observed on some parts of the spectrum. The increase in energy is larger for a stronger current. An explanation for this phenomenon is that interaction between the opposing forces of the waves and the current cause an arising turbulent high frequency motion. The low frequency energy of the spectrum does not change significantly, making it unlikely that the high frequency energy increase is caused by current induced of wave breaking. Overall it has to be concluded that an opposing current increases the wave steepness and enhances the nonlinear growth of higher-harmonic components. This a shoaling alike effect and thus logically leading to accelerated breaking of the wave.

2.3. Wave height distribution

The wave height at deep water is Rayleigh distributed. In shallow water, the number of larger wave heights decrease, e.g. by wave breaking. Then the distribution of waves is well represented by a Composite Weibull distribution (Battjes & Groenendijk, 2000). This is a Rayleigh distribution of which the tail, above a certain threshold value (H_{tr}), is replaced by a Weibull distribution. The threshold value is also called the transitional wave height. The Composite Weibull distribution is shown in Figure 2-1. The formula for the Composite Weibull distribution is given in Equation 2.

Equation 2

$$p(H) = Pr\{\underline{H} \leq H\} = \begin{cases} p_1(H) = 1 - exp\left(-\left(\frac{H}{H_1}\right)^{k_1}\right), & H \leq H_{tr} \\ p_2(H) = 1 - exp\left(-\left(\frac{H}{H_2}\right)^{k_2}\right), & H \geq H_{tr} \end{cases}$$

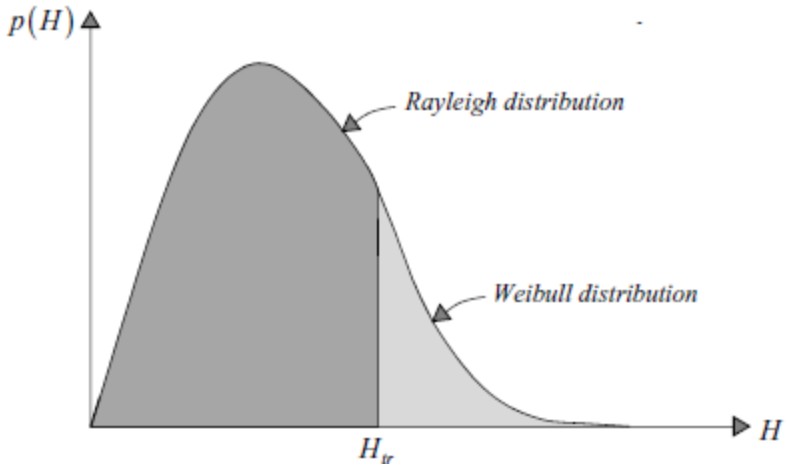

Figure 2-1. The Composite Weibull distribution (Holthuijsen, 2007)

In Equation 2 the exponents k_1 and k_2 are shape parameters of the distribution. They determine the curvature of the corresponding part of the distribution. Since the wave height distribution below H_{tr} has a Rayleigh distribution, it is a pre-given that $k_1 = 2.0$. In the point model, the solution that is suggested by Battjes & Groenendijk, k_2 has the value 3.6. H_1 and H_2 are scale parameters. H_{tr} can be approximated by Equation 3. In this equation α stands for the slope of the foreshore and d for the still water depth.

Equation 3 $$H_{tr} = (0.35 + 5.8 * tan(\alpha)) * d$$

Note that continuity of the wave height distribution places a continuity condition on the Composite Weibull distribution, see Equation 4.

Equation 4 $$p_1(H_{tr}) = p_2(H_{tr})$$

3. Methodology

For this research field measurements are executed. These field measurements were part of a larger measurement campaign. In section 3.1 an extended description of the measurement area and the measurement campaign is given. As mentioned in previous sections, WRD's are used for the measurements. More on the type of WRD used, the WaveDroid, is given in section 3.2. Section 3.3 handles the way to deal with the differences in the frame of reference, that is aimed to execute in a later stage of the research.

3.1. Description of the measurement campaign

3.1.1. Local environment

The *Drifters in SEAWAD field campaign* was executed as a part of larger field work, executed by different organizations and companies. At about the same time measurements were executed to learn about sediment transport, bathymetry and ecology in the area. The *Drifters in SEAWAD field campaign* focussed the research on the intra-wave sediment transport.

The field campaign took place in one of the tidal inlets of the Wadden Sea: the Amelander Zeegat, between the Wadden Sea barrier islands Ameland and Terschelling. This is an area that is complicated in terms of hydrodynamics and morphodynamics, as is elaborated on below. It is one of the points of interaction between the North Sea and the Wadden Sea.

The North Sea has a tidal system on the scale of the sea itself with two amphidromic points and tidal waves travelling around them. One of the points is located north of the Netherlands and one is located west of the Netherlands. A tidal wave travels in approximately 9 hours from South to North along the Dutch coast, from the border with Belgium to the one with Germany (Bosboom & Stive, 2012). Along the coast of Holland this tidal wave motion is almost 2-dimensional and alongshore orientated.

The Wadden Sea coast consists of a number of barrier islands with at the onshore side of them several large tidal basins at the onshore side of them. The tidal basins together form the Wadden Sea. The tidal prism of the entire Wadden Sea is $2.8*10^9$ m^3. With a volume of almost $0.4*10^9$ m^3 the Amelander Zeegat covers circa 14 % of this tidal prism (Duran-Matute, et al., 2014). During each tidal wave this volume of water flows through the tidal inlets into the basin. The main direction of that flow is perpendicular to the coast line of the barrier islands.

When the tidal wave passes the Wadden Sea coastal area the alongshore flow interferes with the tidal flow perpendicular to the coast line. The result is a complicated 3-dimensional flow. The 3-dimensionality of the flow induces a lot of processes to play a role in the coastal dynamics. In the tidal inlet, the tidal current can spatially vary on scales of several kilometres. Since the sea close to the inlet is shallow, the influence of the wind on the water gets relevant. This further complicates the situation.

Influenced by currents and waves, the bathymetry of the inlet is highly variable. This variability is both spatial and temporal. The current bathymetry consists of a couple of channels and shallows alternating in the alongshore direction. Over the years the channels and shallows shift to the east. This changes the bathymetry and consequently it changes the hydrodynamics and morphodynamics of the inlet.

In the research area the tidal amplitude is just over 2 m. The wave height is usually under 1 m with a couple of days every month that wave heights are larger, up to wave heights of several meters during stormy periods. The wind speed is usually between 5 and 10 m/s but peaks up to 20 m/s can be measured. (Rijkswaterstaat, 2017)

3.1.2. The Drifters in SEAWAD Field Campaign

The *Drifters in SEAWAD field campaign* measured waves and currents. During this field campaign current drifters and wave-resolving drifters were deployed. This research focusses on the results of the latter. For more explanation on the WRD's, see section 3.2. The drifter experiments ran from the 28th of August till the 13th of September of 2017.

The drifters have been deployed in the area of the Akkepollegat, one of the channels of the Amelander Zeegat. The measurement area has a size of approximately 1500 x 800 m and is located at the off-shore slope of the ebb tidal delta. The water depth in the area ranges from approximately NAP – 3 m to NAP – 9 m. In the measurement area also 2 measurement frames and 8 pressure sensors were present, see Figure 3-1 and Figure 3-2. The measurement frames and pressure sensors are fixed frames of Rijkwaterstaat to collect data on wave and current characteristics. The frames and sensors are on fixed on their location. In this research the data is used to compare with the resulting data from the WRD's.

Measurements consisted of individual deployments of the WRD's. The deployments went as follows.

- Start of deployment. The WRD's were deployed at the edge of the measurement area where the tidal current entered the area. This edge could be determined based on the knowledge of the tidal motion.
- Deployment. The deployed WRD's were tracked during their deployment time.
- End of the deployment. When the WRD's were about to exit the measurement area they were taken out of the water. Subsequently they were transported back to the area where the deployment started, to be redeployed. Between two consecutive deployments the obtained trajectories were assessed. If regard favourable for the results, the possibility existed to adjust the location of the start of the deployment.

This is procedure was repeated during an entire tidal wave. Simultaneously with the WRD's the current drifters were deployed in the same way as the WRD's.

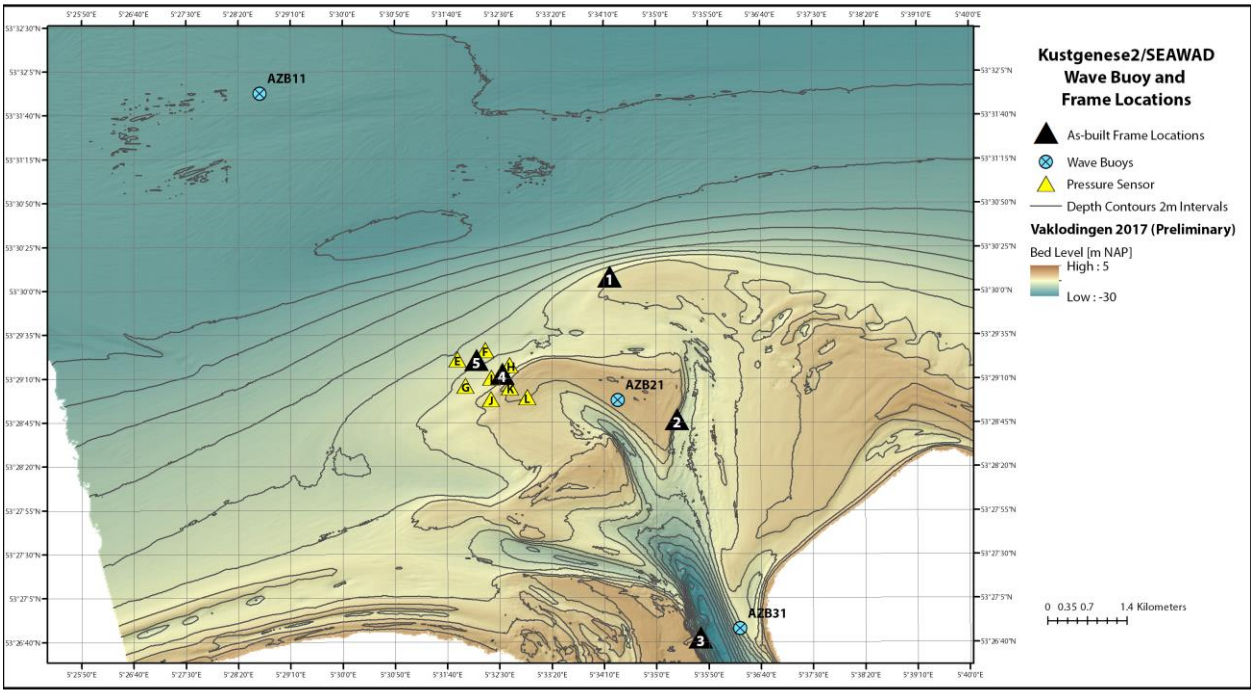

Figure 3-1. Location of measurement devices SEAWAD in the Amelander Zeegat (Courtesy of S.G. Pearson, 2017)

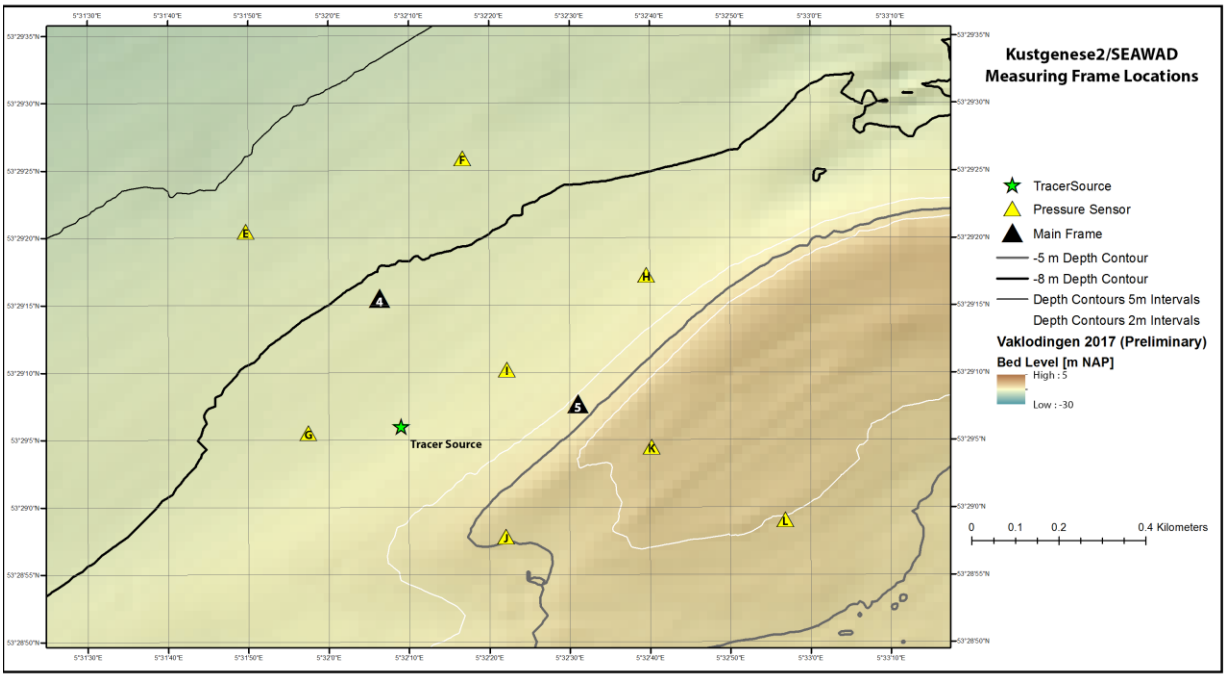

Figure 3-2. WRD deployment area with measurement devices (Courtesy of S.G. Pearson, 2017)

The deployments of WRD's have taken place between the 1st of September and the 10th of September 2017. Measurements were made with deployments in different sea states: Both ebb and flood, wave heights ranging from almost zero to more than one meter and with wind coming from directions between south and north west.

Because the first days of measurements outdated software was used in the measurement devices, the data series of the first days of measurements contain significantly more measurement errors. This research is therefore mainly based on the data collected on the 9th of September. This gives a total of 18 individual WRD deployments divided into 6 consecutive deployments of 3 WRD's.

The times of the deployments of the three WRD's are displayed in Table 3-2. The conditions under which the deployments took place are displayed in Table 3-1 and in Figure 3-3. The information on the conditions is gained from measurement stations from Rijkswaterstaat. Because the Rijkswaterstaat measurements are retrieved from a limited number of locations, the location where this information comes from deviates from the measurement location. The choice for representative station is based on water depth and fetch (concerning the main wind and wave direction). Station *Schiermonnikoog Westgat Buiten* is the best representative measurement station. It is at the outer delta of the inlet between Ameland and Schiermonnikoog, approximately 25 km east of the measurement area. From *Station Schiermonnikoog Westgat Buiten* no wind data is available. For the wind data *Station Terschelling Noordzee* is the best representative station. This station is located a few kilometres offshore of Terschelling, halfway the island. For both this station and the measurement area, the wind comes from the open sea for approximately the same wind directions and it also comes from land areas for approximately the same wind directions.

Figure 3-3 shows with the water level clearly the asymmetry of the tidal wave. High water slack occurred at approximately 13:00 h. Measurements cover therefor both ebb and flood tidal current. The first 3 deployments were before 13:00 h during flood tidal current and the last 3 deployments after 13:00 h during ebb tidal current.

Table 3-1. Conditions during WRD deployments, between 09:00 and 17:00 9 September 2017 (Rijkswaterstaat, 2017)

	Wave height [m]	Wind direction [-]	Wind speed [m/s]
Representative station	Station Schiermonnikoog Westgat Buiten	Station Terschelling Noordzee	Station Terschelling Noordzee
Conditions	0.5 to 0.7	South-West turning to North-West	3 to 8

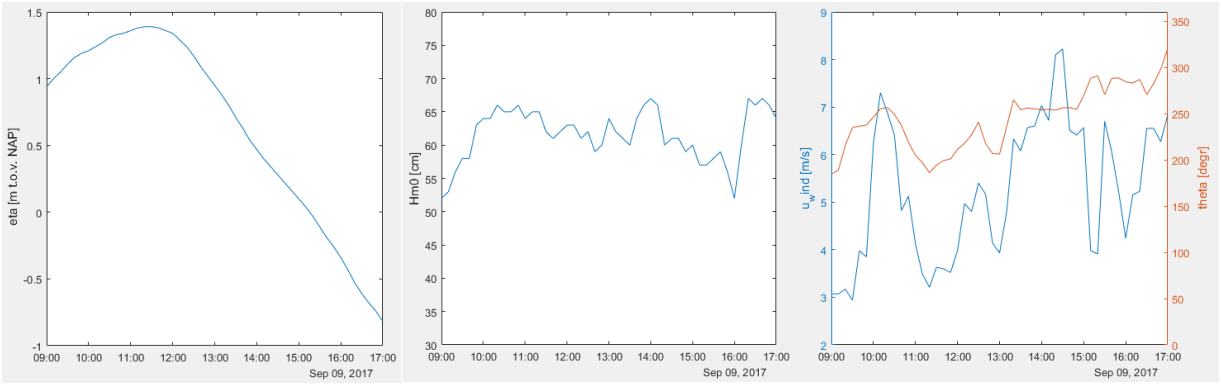

Figure 3-3. Water level at Terschelling Noordzee (left), wave height at Schiermonnikoog Westgat Buiten (middle), wind speed and wind direction at Terschelling Noordzee (both right) as observed during deployment (Rijkswaterstaat, 2017)

Table 3-2. Deployment times sorted by grouped WDR deployment

Deployment no. [-]	Time of deployment [hr:min]	Time of retrieval [hr:min]	Time in the water [min]
1	9:35	10:05	30
2	10:30	11:05	35
3	11:35	12:25	50
4	13:35	14:05	30
5	14:35	15:20	45
6	15:50	16:25	35

3.2. Wave resolving drifters

For the measurements in the field campaign WaveDroids are used. A WaveDroid is a type of wave buoy that is designed to operate moored. A system of a mooring line with floaters and weights allows the WaveDroid to move over some distance in the horizontal plane without being forced to topple over by the mooring line. A sufficiently heavy chain, attached to the bottom plate, stabilizes the WaveDroid. A moored example of the WaveDroid is displayed in Figure 3-4.

For the field campaign the WaveDroid is used unmoored. That is previous described moored use, without the use of the mooring line with floaters and weights. With this unmoored use, the WaveDroid is used as a WRD. This field campaign is the first time the WaveDroid is used unmoored. The unmoored use means that all data excluding GPS measurements represent waves in a Lagrangian frame of reference with the WaveDroid as the origin of the frame of reference.

The WaveDroid itself consist of a plastic cylindrical housing with an external antenna on top of it. The WaveDroid is kept afloat by a ring-shaped floater that is strapped around it.

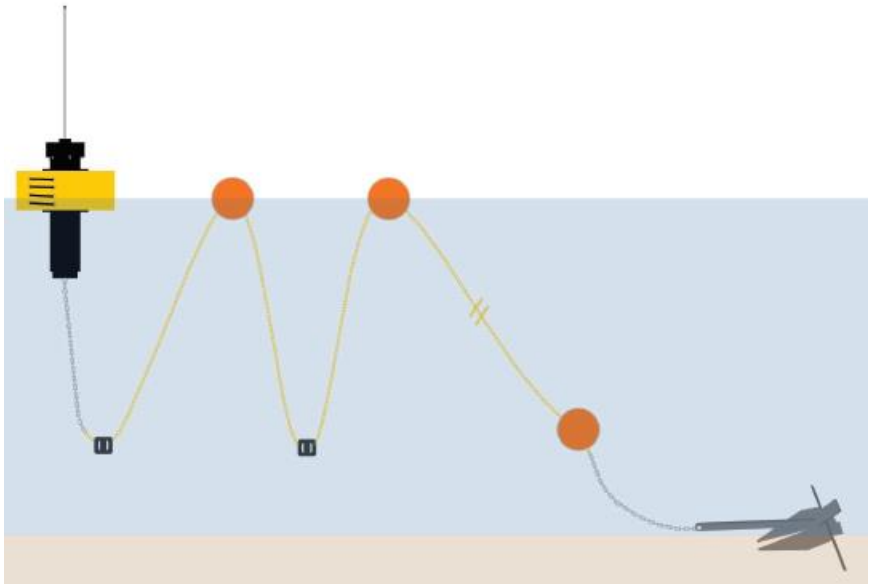

Figure 3-4. WaveDroid, typical deployed configuration (Wavedroid, 2017)

The actual measurement device is a smartphone that contains the required sensors for measurement and with the WaveDroid app installed on it. The smartphone measures accelerations with its accelerometer, the pitch and heave and roll with its gyroscope, the magnitude of the magnetic field with its magnetometer and the geographic position on earth (the longitude and latitude of the position) with its GPS. All measurements are done with a sampling frequency of 5 Hz. GPS data is send every 40 seconds. It is experienced that at the moment of this sending the updating of the timestamp is interrupted, causing an error in the time series. During data processing there is a check on the existence of such an error.

The raw data from the WRD measurements contains the motions of the WRD expressed in translational accelerations with respect with respect to the current position of the WRD (from the accelerometer), rotational accelerations (from the gyroscope) and position with respect to the magnetic north (from the magnetometer). These quantities are not very conceivable and they do not display the WRD motions in a way that is useful for this research. The raw data from the WRD measurements must be translated in quantities that are representing motions in a more conceivable way. This means translation into for instance orbital displacements and conversion to another frame of reference. More information on this translation is given in section 4.1.1.1.

3.3. Frame of reference

In the previous section it is stated that WRD's do measure in a Lagrangian frame of reference. It is useful to be able to compare the wave signals from the WRD with other measurements or with existing knowledge on the subject. Hence, it is useful to transform the data from the WRD into a Eulerian frame of reference.

A first step of this translation is done by obtaining the wave orbital motion from the data (see section 4.1.1.1). After this step there is no tilting and rotating of the WRD in the wave data anymore. Information on tilting and rotation of the WRD is not useful in this research.

According to Equation 1, for the remainder of the translation information on the wave length (represented by k) and the current velocity (U_n) is needed. U_n is measured in the *Drifters in SEAWAD Field campaign* with the current drifters. Wave number k is gained by applying the dispersion relation. The dispersion relation gives the relation between the frequency ω and the wave number k (Peregrine & Jonsson, 1983). The dispersion relation is given in Equation 5. In this relation d stands for the water depth. With the use of U_n and k, the comparison between the use of different reference frames can be completed.

Equation 5 $$\omega = \sqrt{gk\ tanh\, kd} + kU_n$$

4. Results

The raw data that result from the measurements is processed and analysed, in different subsequent steps. The first step is to convert the raw data into more understandable motion-representing quantities, like displacement. This is reported in section 4.1.1. The second step is to look into the observed errors, to understand their origin and to eliminate them, see section 4.1.2. In processing a selection of data takes place, separating data that is not useful in the continuation of this research from the data that is useful. Both steps are aimed at preparing the data for analysis and interpretation of the wave field. The last step is to analyse and interpret the data in terms of represented waves, see section 4.2.

4.1. Measurement results

The measurement campaign resulted in data series of 18 WRD deployments. Figure 4-1 displays all WRD trajectories that are measured. The WRD trajectories are shown in red, with green dots indicating the starting position of each individual resulting data file. The yellow dots and the black circles indicate the pressure sensors and measurement frames respectively.

Some of these data series are split in several sections during processing, resulting in 26 individual data series, see section 0. Data sets that got very short after this processing step, are filtered out directly. All data series are displayed in Table 4-1. The names of the data series contain info that is ordered as follows: WD00[ ]_d[ ]_s[ ]. After *WD00* the number of the WaveDroid is placed, after *d* the number of the deployment and after *s* the number of the data section. Note that the count starts at zero for the deployments and sections. Table 4-1 also gives per deployment the length in time. The sampling frequency was 5 Hz, resulting in 5 data per second of drift.

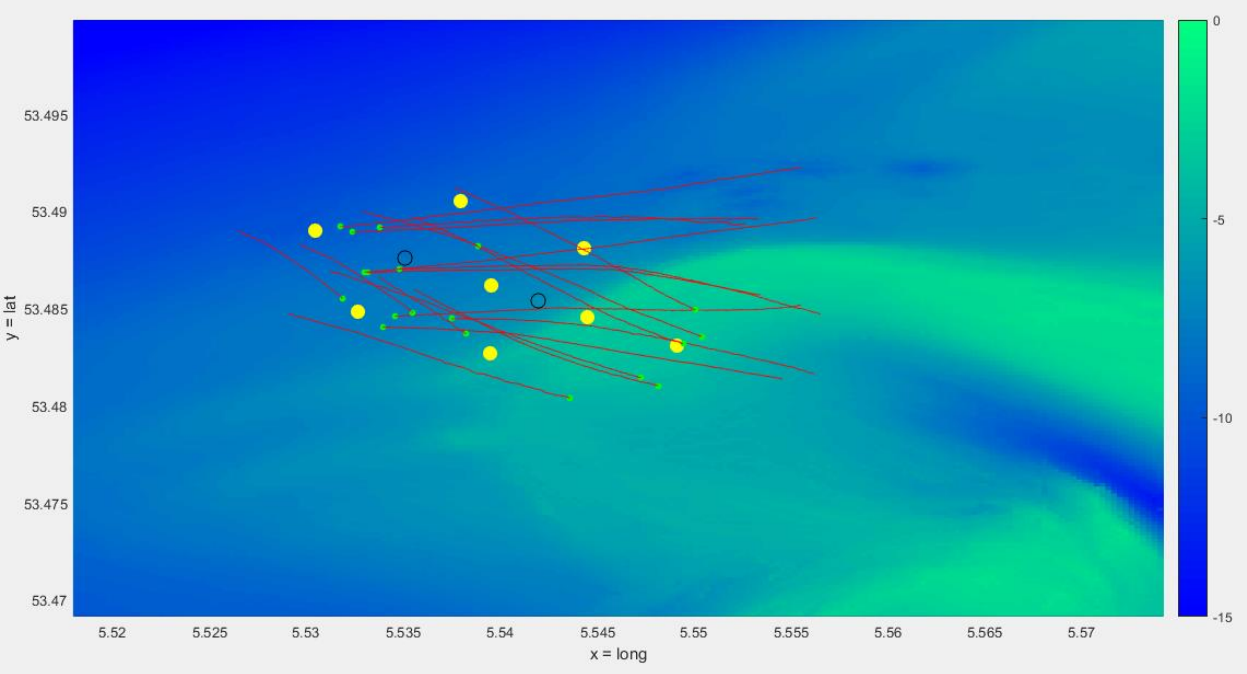

Figure 4-1. WRD trajectories (red lines) with indication on starting position of data set (green dots), locations of the measurement frames (black circles) and the locations of the pressure sensors (yellow dots), on 9 September 2017 between 9:00 and 17:00 h. The bottom level is shown by the coloured scale.

4.1.1. Preparatory raw data processing

The raw data results from the measurements with the WRD's is processed. The processed data is the data that is used in further analysis. The processing consists of a number of processing steps that are elaborated on in this section.

4.1.1.1. Data conversion

The signals of the measurement devices (the accelerometer, the gyroscope and the magnetometer) are converted into more conceivable motion representing quantities, e.g. accelerations. The raw data give motion in three orthogonal directions. These directions span a frame of reference with the smartphone as origin. This conversion is done as follows. With the data of the accelerometer and the gyroscope the acceleration in the x,y,z-space are calculated. The x,y,z-space is the frame of reference with the WRD as origin. Note that the x,y,z-space is moving and rotating along with the WRD. First the rotation around the x- and y-axis is filtered out. To reconstruct the direction of the moving WRD, the rotation around the z-axis is not filtered out. The data now represents a vertical positioned WRD that is moving with the surface elevation and the current. This data still shows the motions just as accelerations, not yet as velocities or displacements.

The accelerations are subsequently converted into velocities and displacements by single and double integration respectively. The resulting motion quantities are still representing the motion of a vertical positioned WRD in an x,y,z-space.

Finally, using the data from the magnetometer, the accelerations, velocities and displacements are displayed in a n,w,η-space. This is a geographical frame of reference with north (n) and west (w) for the horizontal directions and η for the vertical direction.

4.1.1.2. Frequency filter

Not all harmonic wave components are in the area of interest, because the waves are either too short or too long. Approximately all energy of waves forced by wind (wind sea waves and swell waves) have energy in frequencies between approximately 0.05 Hz and 1.0 Hz, with also minor influence of the wind in frequencies above 0.2 Hz (Munk, 1950). The currents can be found in the harmonic components with a very low frequency. The harmonic components that are not in the area of interest, the components with frequencies outside the band between 0.05 and 1.0 Hz, are filtered out.

In the application of the frequency filter information is lost. This creates discrepancies between the wave field that can be reconstructed from the data before and after processing. After filtering the data on displacements represent only wave induced displacements. It is no longer possible to reconstruct the trajectory of the deployed WRD with this data. To obtain the trajectory, the GPS data must be used.

4.1.1.3. Time step correction

Every 40 seconds, the measured data from the WRD is transmitted. Data transmission has interfered with the storage of the data, causing errors in time stepping. These errors show a leap in the update of the time stepping. The magnitude of error varies from 0.2 seconds (a single time step) till more than a second. In the time stepping a leap is balanced by a number of measurements at approximately the same time. This number equals the number of time steps that fit in the accompanying leap, when using the sampling frequency. For instance, if the time series skips 0.6 seconds, the next 3 time measurements are stored at approximately the same time instant. The data on the measurement time steps itself is largely corrected with this balancing. However, the discontinuity causes large errors in processing, for instance in integration.

To enable useful analysis of the data, the errors are removed. The small errors, the ones with a length shorter than 0.5 seconds, are interpolated, resulting in a time series with an even sampling frequency of 5 Hz. The errors larger than 0.5 seconds are cut out of the data series, splitting a data series in multiple individual data series.

Due to the splitting of the data series, some of the data series cover a short time frame. Since the series that are shorter than 10 minutes turn out to give bad and unreliable results, they are considered to be of no value, limiting the number of useful data series to 19. They are marked in grey in Table 4-1. A more extended overview of the data and how they are treated and change in different processing steps is given in Appendix A.1.

Table 4-1. Overview of data series with their names and covered length in time ordered by WaveDroid and deployment, with the data series that are judged to be too short marked in grey.

	Deployments WaveDroid 1 [-]	length [min:s]	Deployments WaveDroid 2 [-]	length [min:s]	Deployments WaveDroid 3 [-]	length [min:s]
Deployment 0	WD001_d0_s0	30:00	WD002_d0_s0	30:00	WD003_d0_s0	30:00
Deployment 1	WD001_d1_s0	03:15	WD002_d1_s0	35:00	WD003_d1_s0	28:16
	WD001_d1_s1	26:41			WD003_d1_s1	06:42
	WD001_d1_s2	03:01				
Deployment 2	WD001_d2_s0	01:02	WD002_d2_s0	49:00	WD003_d2_s0	49:00
	WD001_d2_s1	47:56				
Deployment 3	WD001_d3_s0	20:00	WD002_d3_s0	20:00	WD003_d3_s0	13:57
					WD003_d3_s1	06:02
Deployment 4	WD001_d4_s0	24:35	WD002_d4_s0		WD003_d4_s0	00:57
	WD001_d4_s1	20:24		45:00	WD003_d4_s1	36:59
					WD003_d4_s2	07:02
Deployment 5	WD001_d5_s0	35:00	WD002_d5_s0	35:00	WD003_d5_s0	35:00

4.1.1.4. Magnetic correction

Every once in a while, the Android operating system does a calibration on the magnetometer and presents this calibrated data as output (Michel, et al., 2015). This calibration causes the data to jump from one value to a not adjacent next value. That leap in the data is not explainable using hydrodynamics. It influences all spatial data resulting from the measurements. A leap like that can be seen as a Heaviside step function. This function can be approached with the use of a Fourier analysis and is filtered out by a magnetic correction. In a Fourier series this erroneous Heaviside step function is represented by a very low frequency harmonic component. This means that with the calibration a very low frequency wave energy enters the wave spectrum. The harmonic components associated with this energy is filtered out, removing the error largely.

The usual moment of applying the magnetic correction is on the raw data, before processing and integration into displacements. The disadvantage of this order is that a small error that can remain after the correction, blows up during integration. This results in erroneous low frequency energy. Another order of processing is to do the magnetic correction after integration. This should minimalize the amount of low frequency error originating from this correction. This order, called the delayed magnetic correction, is new and untested. Further in this report both methods are compared (see section 0.).

It should be noted that in practice the way of filtering out this error follows the same steps as the frequency filter that is described in section 4.1.1.2. However, the reason of filtering is very different. The frequency filter filters out harmonic components that are simply not relevant for this research. The magnetic correction filters out harmonic components that originate from an error. Because of the existence of this difference and of a possible difference in treatment both corrections are mentioned separately.

4.1.2. Correcting data processing

In the first processing steps the raw data from the measurement devices are translated into quantities that are easier to understand, like accelerations. At this point the data still contains errors. The errors must be removed before the data is suitable for wave analysis.

Errors that have been observed in the data are the occurrence of too large amounts of low frequency energy and the occurrence of erroneous large waves. The low frequency energy error is the existence of large amounts of wave energy in the frequency band below 0.1 Hz. Visually observed waves during measurements were in higher frequency regions, around 0.15 - 0.2 Hz (wave period of 5 – 7 s). The large wave error is the occurrence of waves (single waves or groups) with wave heights that are significantly larger than the significant wave height.

Furthermore, it is known that there is a discrepancy between the wave data and the knowledge on wave characteristics, based on the frame of reference used, see section 2.1. The influence of this discrepancy must be investigated. Only than it is possible to know what the result of the data analysis is really meaning. Keep in mind that this discrepancy is no error but a difference between two types of observation.

4.1.2.1. Low frequency energy

The data shows an unusual large amount of energy in the lower frequency regions (f < 0.1 Hz) of the energy density spectra for displacement. The spectra most of the deployments clearly show the erroneous large peak of energy below 1 Hz with its peak around the lower limit of the frequency band of interest (0.05 Hz), see for an example Figure 4-2. This is the case especially in the spectra for horizontal displacement.

Introduction of an error can be partially explained by the magnetic correction on the calibration of the WRD. For the magnetic correction two orders of processing were executed. Figure 4-2 shows the comparison of the results for one of the deployments from both orders. Delaying the magnetic correction clearly reduces the low frequency wave energy. Obviously, the upward displacement is not influenced by the magnetic calibration, hence its spectrum does not change.

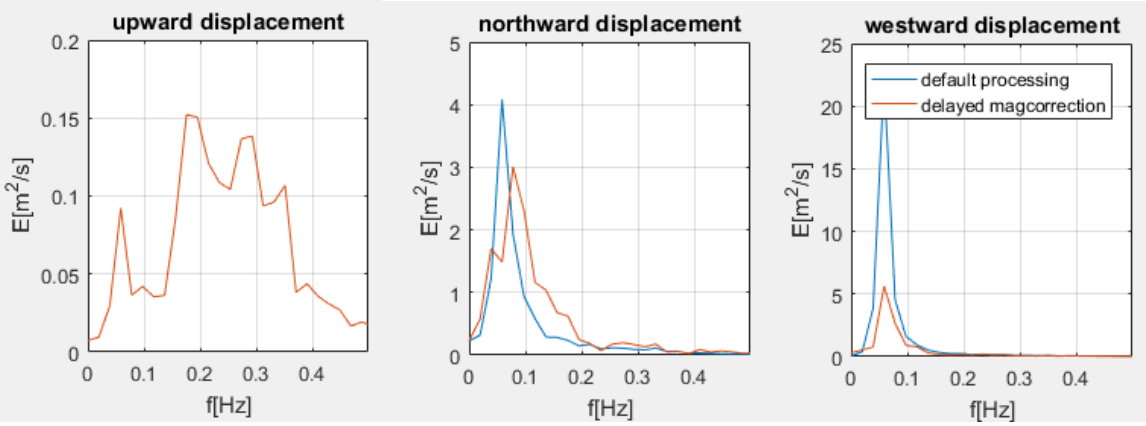

Figure 4-2. Displacement spectra resulting from conventional (default) processing order and the delayed magnetic correction (WD001 d5 so). Both spectra of horizontal motions are influenced in different amounts, the spectrum of vertical motion is not influenced.

The presence of low frequency energy is quantified by computing the variance of the harmonic components with a frequency lower than 0.1 Hz. This upper frequency limit is chosen because the erroneous energy peak is located almost complete below this frequency for all deployments. All calculated values are displayed in one table in Appendix B. The table shows that for the considered cases the effect of the delayed magnetic correction is very diverse: for 18 cases the variance reduces, for 15 cases there is no significant difference and for 5 cases the variance grows.

The different effects on the variance can be explained. The cases with the reduced variance is explained by the reduction of the erroneous low frequency wave motion. The cases where the effect of the delayed magnetic correction is not significant can be explained by the lack of an error due to magnetometer calibration. A possible explanation for cases where the variance is growing can be explained by three different causes. The first cause is the entrance of energy on very low frequency wave motions, caused by the delayed magnetic correction. An example of this entrance of energy can be observed in Figure 4-2. For deployments where the entrance of this energy is large, the variance increases significantly. The origin of energy is not further hypothesized upon. This research does not focus any further on these causes for growing low frequency energy, since most time series do not suffer from it.

It must be concluded that the application of a delayed magnetic correction is favourable for the data in a way that it decreases the low frequency wave energy peak. This means that the data becomes a better approach of a real wave signal. Based on this it is decided to use the data that is processed with a delayed magnetic correction.

4.1.2.2. Erroneous large waves

Most of the data series show erroneous large waves at the start and at the end of each deployment. Some data series also show large waves more halfway the deployment. The errors at the start and at the end of the deployment are likely to originate from the handling of the WRD's during deploying them and taking them out of the water. Other sources for other erroneous waves can be either physical or numerical. Examples of physical errors are close passing of vessels, bypassing of fixed frames or errors in the measurement device. Examples of numerical errors are errors in data storage or deviations originating from the processing. Waves that are too large point at errors in the data and must be removed.

Setting a threshold

A threshold is set to determine which waves must be removed. To set a threshold level an expected wave height distribution is used. The most suitable distribution for near shore wave conditions is the Composite Weibull distribution (Battjes & Groenendijk, 2000). This distribution is closely related to the Rayleigh distribution. (Note that in the context of horizontal wave motion the term wave height might be confusing. It is nevertheless the height of the wave signal that represents the oscillatory horizontal displacement.)

The knowledge of wave height distributions is based on vertical wave motion, but in this research also horizontal wave motions are considered. The water depth over incoming wave height ratio does not change much in the measurement area. This ratio is an indicator of the degree of shallowness of the water, and there for an indicator of the degree of flattening of the deep water circular wave orbital motion. It is assumed that in the measurement area the shape of the orbital motion is approximately equal. Therefor the length of each vertical motion is linked to a horizontal motion with a certain length. Consequently the wave height distribution that is used for a horizontal motion is equal to the wave height distribution of the vertical motion.

The transitional wave height H_{tr}, applied in the Composite Weibull distribution, can be calculated using Equation 3. The slope of the measurement area is approximately 0.004 and the depth is on average approximately 7 m. (This value is an approximation of the weighted average. The larger depth values are given more weight because more than half of the measurement area lays below NAP – 6 m, see Figure 3-2.) Applying this it turns out that H_{tr} is 2.45 m. Waves heights above 1.5 m were rare during measurements and the significant wave height never exceeded 0.7 according to the measurements of Rijkswaterstaat (see Figure 3-3). H_{tr} has is of a value that is larger than the values that are measured. For this case the Weibull tail of a Composite Weibull distribution is of no significant weight and the wave height distribution is well represented by a Rayleigh distribution.

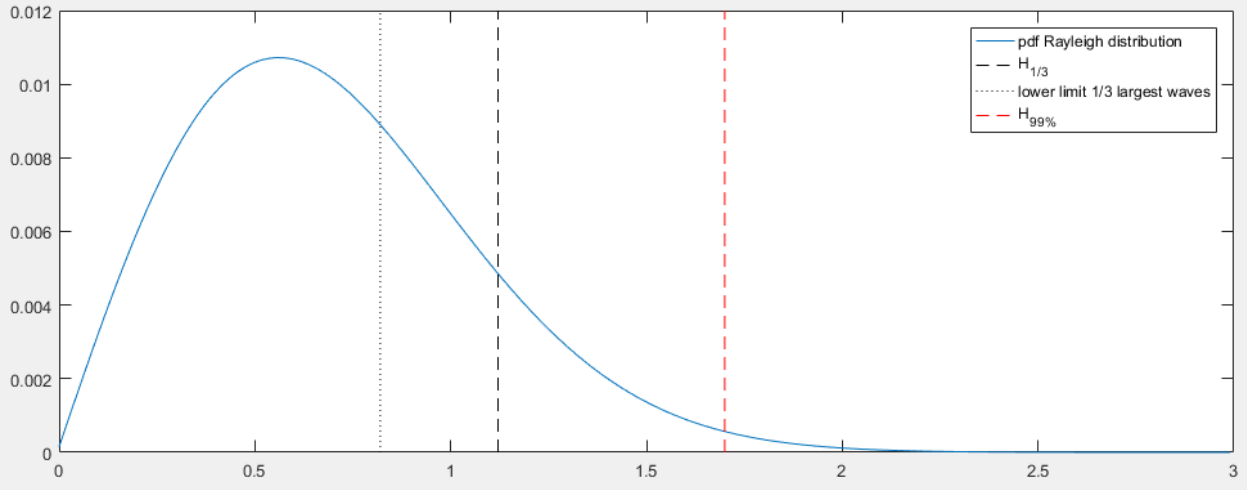

Figure 4-3. An arbitrary Rayleigh distribution with $H_{99.9\%}$ and $H_{1/3}$ indicated

The data sets with the largest length (that of deployment 2) all contain about 750 waves. The data set with the smallest length (3rd deployment of WaveDroid 3) contains just over 100 waves. The threshold wave height is set to be normative in a way for all data sets. The threshold applied is based on maintaining 99.0% of the smallest waves. Since statistically 1 out of 100 waves exceeds the threshold, all data sets can be judged. One wave per 100 waves exceeding the threshold value can be explained by statistics. If the frequency of exceeding waves rises, it is an indication that an error is present in the data that must be filtered out.

The value of the threshold wave height is set using a Rayleigh distribution. A Rayleigh wave height distribution has a characteristic ratio between the significant wave height $H_{1/3}$ and the threshold wave height $H_{99.0\%}$: $H_{99\%}$ is 1.52 times the $H_{1/3}$. Figure 4-3 shows an arbitrary Rayleigh distribution and the locations of $H_{1/3}$ and $H_{99\%}$ on this distribution. The value $1.52*H_{1/3}$ is used as an upper threshold level for wave heights to determine which waves are typed as erroneously large and are removed.

The wave heights during deployment are plotted with the accompanying threshold wave height. Figure 4-4 is an example of such a plot. An overall observation is that the wave motions in the horizontal direction contain way erroneous wave heights than the ones in the vertical direction. It should be noted that the energy density spectra on horizontal motions show more erroneous low frequency energy. The horizontal motion data series are judged to be an insufficient representation of the wave field to start analysing the measured wave field. The table in Appendix A.2. gives an overview of the data that is judged to be erroneous. Removing all data sets that have errors in the horizontal motion, results in a large loss of data and a small set of remaining data. Further correction of the data on horizontal motion will cost a lot of effort before getting at any result. Therefore, it is chosen to narrow the scope of the analysis to the vertical motion only, for the remainder of this research.

Filtering of ends

For the erroneous large waves that are at the ends of the time series and the ones that are somewhere in the middle a different approach is required. At the ends the erroneous waves can simply be cut off, without severely changing the data series. The erroneous waves in the middle cannot be removed without damaging the continuity. This means that this removal results in two smaller data sets or a data set that contains a significant amount of interpolation or waves deformed by processing. An example of the latter one is the cut off of waves at the threshold level. Since interpolation or wave cut-off changes the content of the data this is an unwanted processing method that should only be used if other methods do not lead to useful data sets.

The first filter applied on large wave heights is the Rayleigh-based filter that is applied on both the ends of the series. This is simple since it only shortens the data series. Figure 4-4, Figure 4-5 and Figure 4-6 show the application and effect of this filter. The removal of the erroneous waves has a positive effect on the remaining low frequency energy that is present in the wave signal as hypothesized in the previous section, see Figure 4-5. The effect of this is further quantified using the variance in Appendix B. Figure 4-6 shows the occurrence of wave heights in a single deployment with the best fitting Rayleigh distribution for the data set in one plot. The measured wave heights show a nice fit, already before filtering, but even more after. The display of the presence of large waves match with the previous stated hypothesis that there are too much large waves in the data sets left.

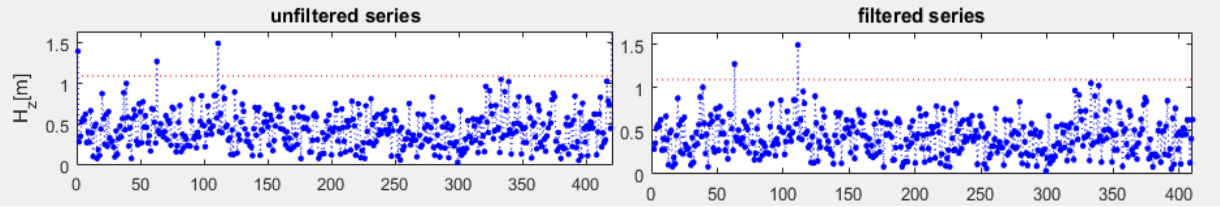

Figure 4-4. Application of a Rayleigh based filter on the ends of the data series on the wave height, with in red indicated the threshold wave height (WD001_d4_s0).

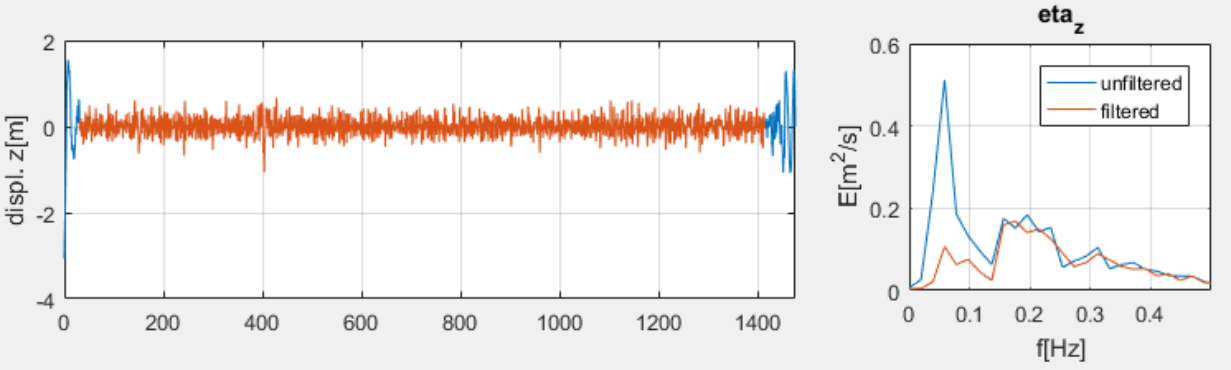

Figure 4-5. The effect of the filtering of large waves at the start and end of the data. The left plots display the time series and the right plots display the energy spectra (WD001_d4_s0).

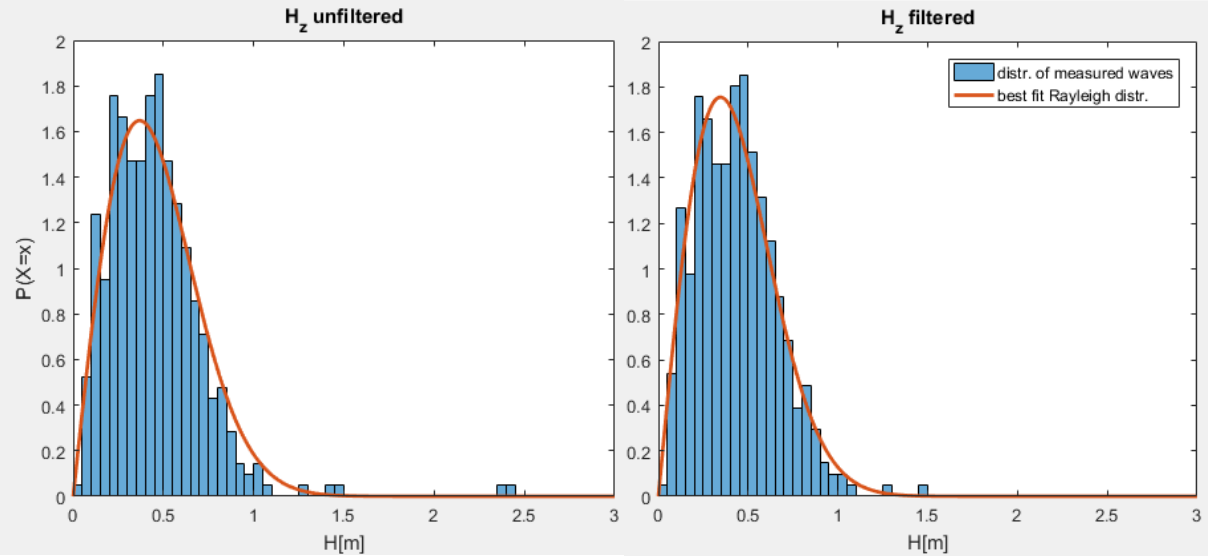

Figure 4-6. The normalized occurrence of wave heights in a deployment compared with the best fitting Rayleigh distribution for a data set of which the ends are not filtered (top three plots) and the ends are filtered (bottom three plots).

Filtering manually

The data still contains errors halfway the data series, that must be filtered. Erroneous wave heights are outliers that are clear extreme values deviating from the bunch and exceed $H_{99\%}$. More than 1 outlier per 100 waves in a data set is not statistical explicable. Single or grouped outliers can be easily cut out of the data, therewith splitting or shortening the time series. Outliers spread throughout the time series are hard, if not impossible, to remove when a part of the dataset must be remained to analyse. Time series with too much outliers do not contain a useful information bin and are discarded.

The second filter applied on large wave heights is taking care of the observed errors. This filter is a manual removal of the data that is judged to be erroneous, based on previous analysis. Manual removal means that for all data sets is determined what parts are kept and what parts are removed. The table in Appendix A.3. displays what parts of the wave series are considered erroneous and are therefore removed.

4.1.2.3. Data selection

From the processed data a selection is made to analyse. There are two reasons to make this selection. First of all, it is of more value to analyse correct data than analysing much data. Hence, the data about which the least doubt exists whether it still contains minor errors is chosen. This choice is made based on analysis of the spectra, the wave height distributions and the time series of the surface elevation and the wave height. Second, the handpicking enables to choose data that is nicely distributed in time, to consider both deployments during ebb and flood.

Furthermore it turns out that the some of the time series still contain low frequency energy. Despite the application of a frequency filter, a delayed magnetic correction and a filtering of large wave heights. An example of this error still present is given in Figure 4-7. Because the correctness of data sets containing this error is doubtful, they are removed.

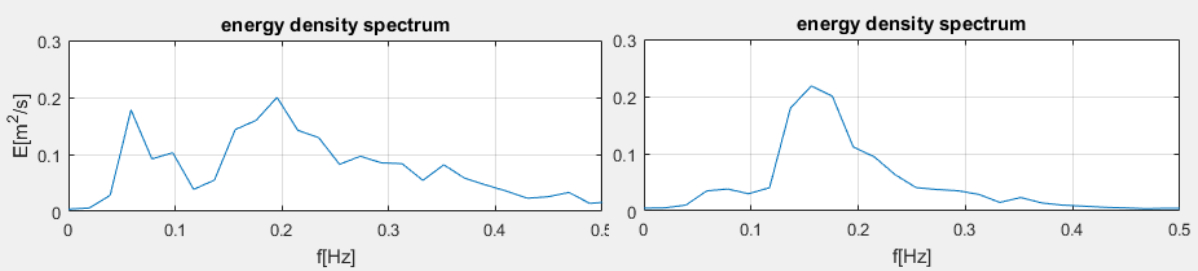

Figure 4-7. Energy density spectra after processing. Left a spectrum still containing low frequency energy (WD001_d4_s1) and right a spectrum cleaned from low frequency energy (WD002_d1_s0).

The final selection of data consists of 6 deployments. The data selection is shown in Table 4-2. The first three deployments were during flood and the last three during ebb. The selected data is used for analysis and interpretation.

Table 4-2. Overview of the data series selected for further analysis

	Deployments WaveDroid 1 [-]	length [min:s]	Deployments WaveDroid 3 [-]	length [min:s]
Deployment 0	WD001_d0_s0	29:15	WD003_d0_s0	18:15
Deployment 1				
Deployment 2	WD001_d2_s1	46:45		
Deployment 3	WD001_d3_s0	18:43	WD003_d3_s0	13:52
Deployment 4	WD001_d4_s0	17:17		
Deployment 5				

4.2. Data analysis results

The data selected from the processed data is analysed to get insight in the wave conditions as they were measured by the WRD's. The trajectories of the selected deployments are shown in Figure 4-8. In this figure the distinction between the deployments during flood and ebb is clear. The deployments during flood are the ones going from west to east and the deployments during ebb are the ones going from south-east to north-west. The plot shows that the directions of the current during ebb and the current during flood are not the opposite of each other. The latter is also displayed in Figure 4-1, be it in a less clear way due to the large amount of data.

The trajectories in Figure 4-8 that enter the shoal during deployment show a curvature. This curvature can also already be observed in Figure 4-1. The phenomenon of a current that is deflecting when it experiences a change in water depth is resembles the phenomenon of wave refraction. The fact that the trajectories of the WRDs show refractive behaviour, can be indicating that the wave direction is of influence on the current direction. (Based on theory it can be assumed that wave refraction takes place over the shoal.) This hypothesis is not proved and left open for further research.

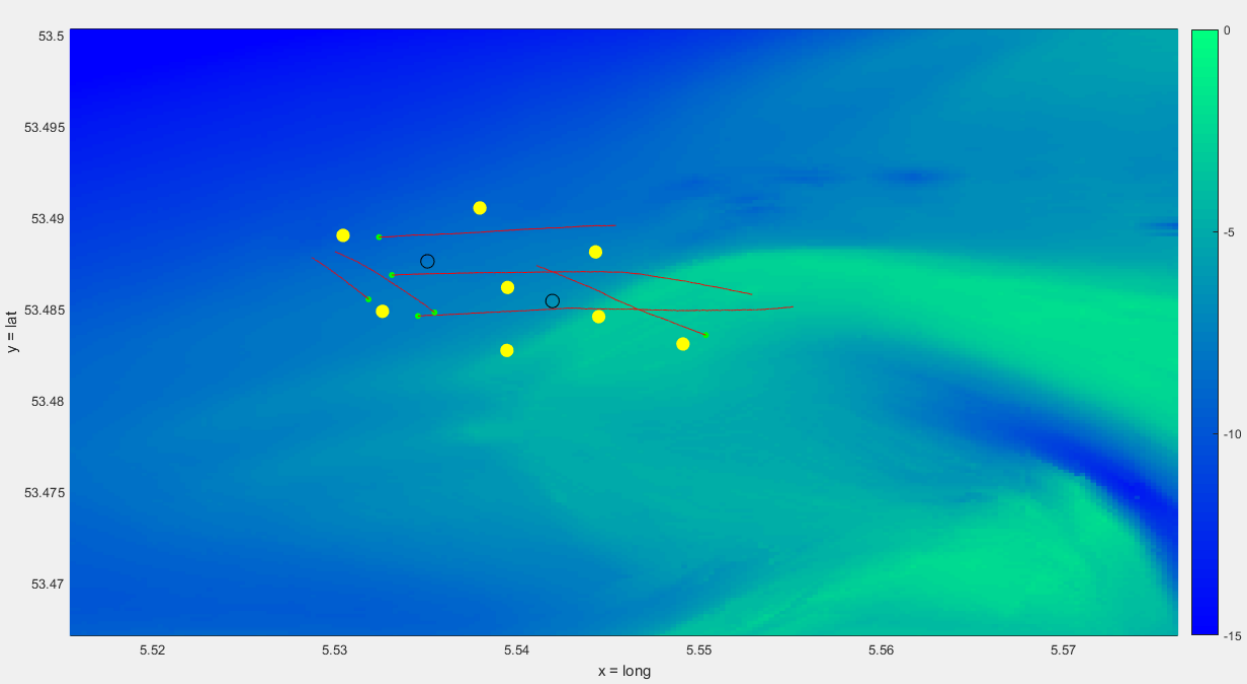

Figure 4-8. Trajectories of the selected WRD deployments (red) with indication on starting position of data set (green), locations of the measurement frames (black circles) and the locations of the pressure sensors (yellow).

4.2.1. Wave-by-wave analysis

A wave-by-wave analysis is executed to get a view on the temporal and spatial evolution of the wave heights and the wave periods during the deployments. The analysis makes it possible to relate variations in the wave characteristics to different locations in the measurement area and different environmental conditions (see Figure 3-3).

The first step of the wave by wave analysis is an analysis on temporal variations. Figure 4-9 and Figure 4-10 show the temporal evolution of the wave heights and wave periods during the day of deployments. The trend lines show the evolution of the significant wave height for the wave height and the evolution of the average period for the wave period. The trend lines are obtained by calculating the significant wave height value and the average wave period value respectively for a block of 60 waves, that is a timeframe of approximately 5 minutes. This value is then ascribed to the wave that is halfway the timeframe.

The trend lines show a decrease in wave period during the day. The wave height does not decrease during the day. Decreasing wave periods, without a decreasing wave height indicate a wave steepening. A possible explanation for this is the gradual change from wind waves and current that are aligned to wind waves and current that are opposed. The latter one causes wave shortening which causes wave steepening.

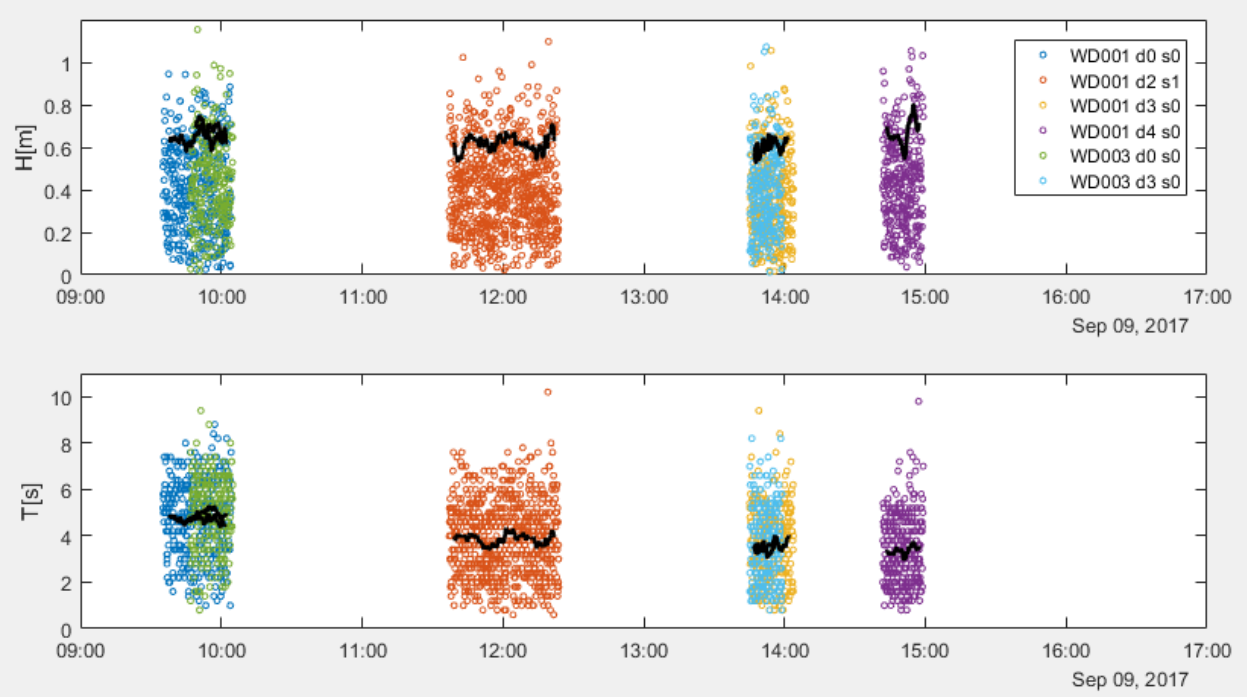

Figure 4-9. Temporal evolution of the wave height (top plot) and the wave period (bottom plot). Each deployment is shown in a different color and the trends per deployment are indicated by black lines.

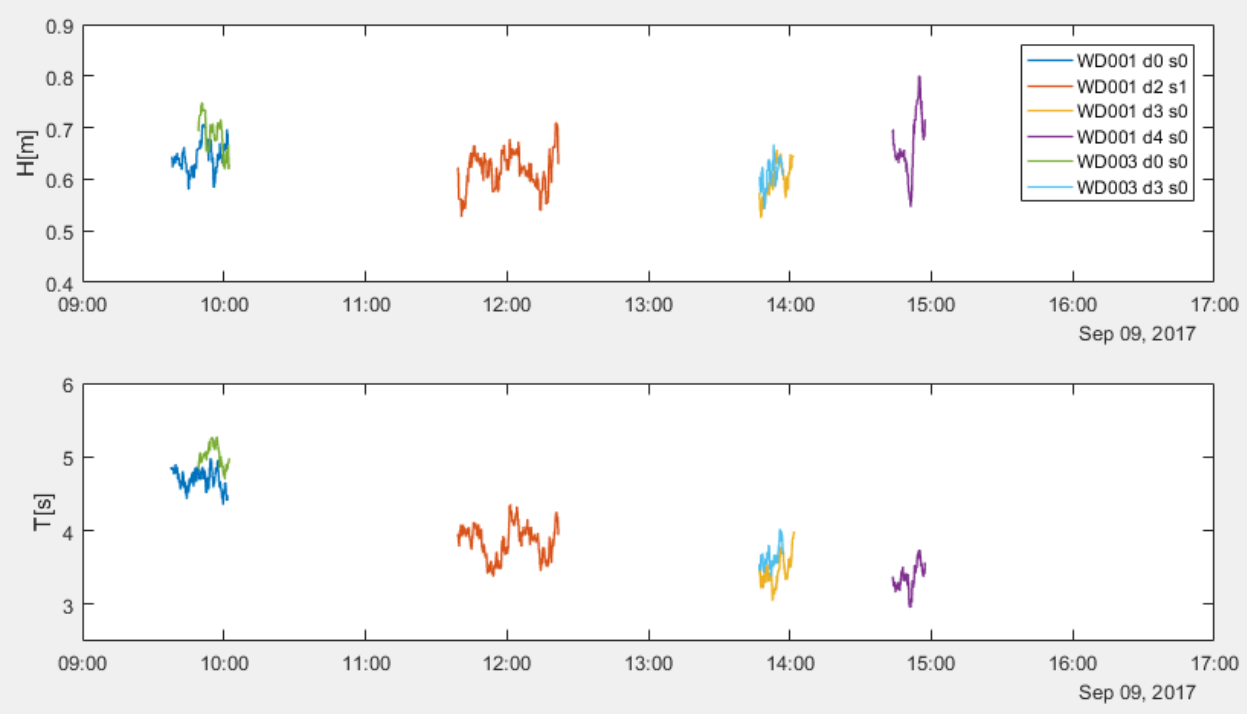

Figure 4-10. Trend lines of the temporal evolution of the wave height (top plot) and the wave period (bottom plot). Colours are matching the colours in Figure 4-9.

Another observation is the presence of similarities between deployments that happened at the same time. This is displayed with a plot that is zoomed in on the trends of the results of the wave-by-wave analysis of deployment 3, see Figure 4-11. The plots of different WRDs show similar tendencies. This is a confirmation in the correctness and relevance of the processed measurement data. The plots of different WRDs show small deviations. These show the magnitude of the influence of spatial variations, for instance rotational flow or bathymetric variability. The wave height of two different deployments deviates up to 0.1 m and the wave period up to 0.5 s. It can be concluded that spatial variability is of influence on wave characteristics.

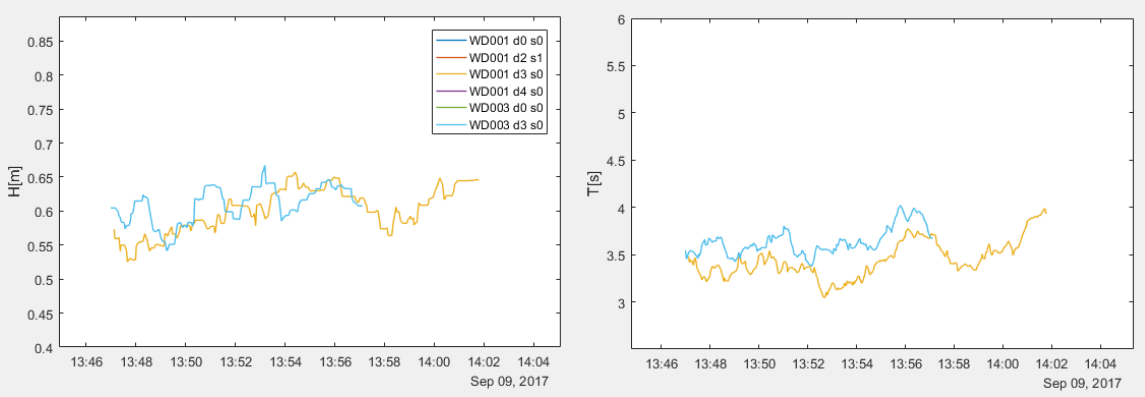

Figure 4-11. Trend lines of the temporal evolution of the wave height (top plot) and the wave period (bottom plot), zoomed in on deployment 3.

A following step in the wave by wave analysis is a more thorough look into spatial variations. The evolution of the significant wave heights is displayed on the wave trajectories, see Appendix 0. Two representatives plots of Appendix 0 are given in Figure 4-12. The plots show a minor decrease in wave height for deployments that travel over the shoal at the south east end of the measurement area. That theory of shoaling states that the wave height of a wave travelling into shallow water grows. The observations on wave heights above a shoal violates the theory of shoaling.

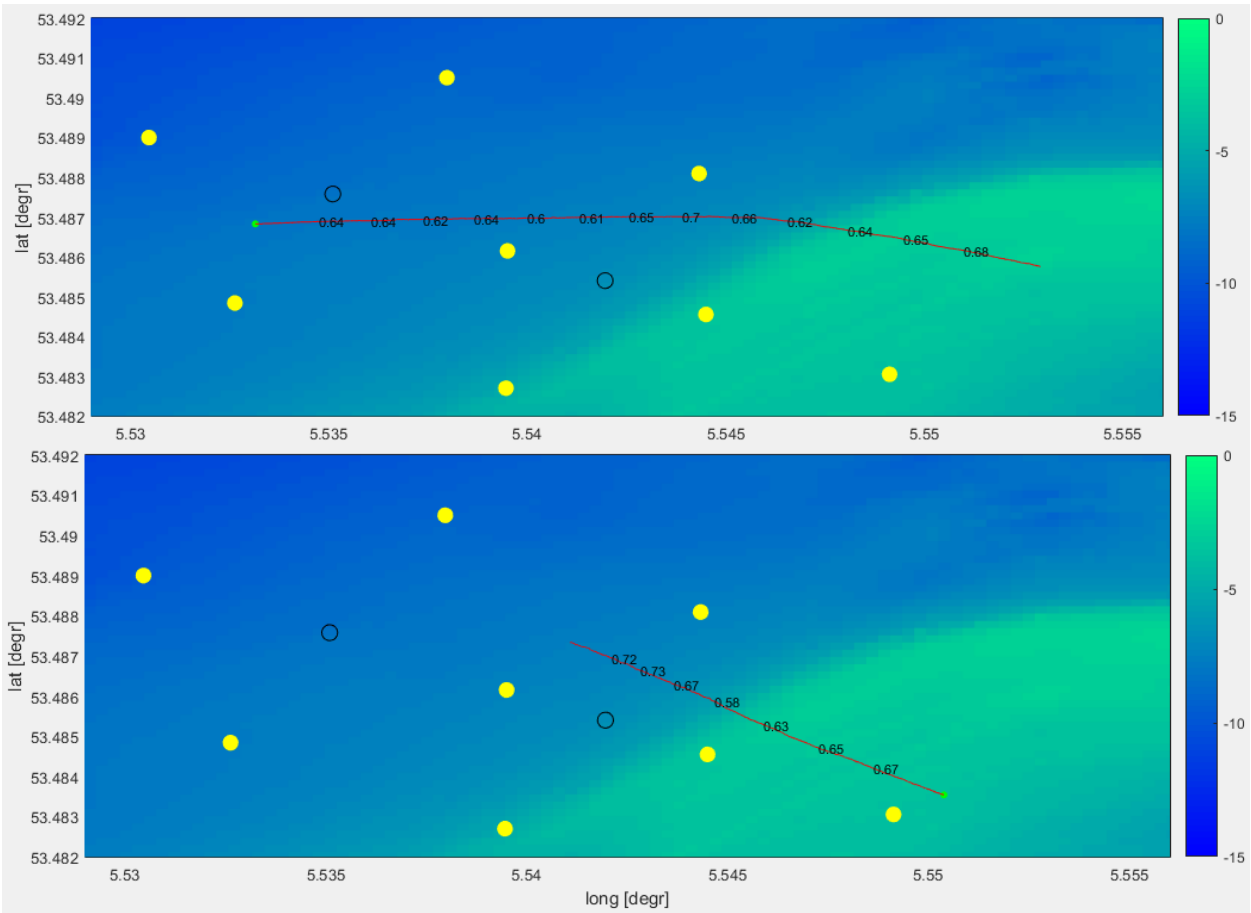

Figure 4-12. Evolution of the significant wave height of two different deployments, the top one during flood (WD001_do_so) and the bottom one during ebb (WD001_d4_so).

4.2.2. Spectral analysis

A spectral analysis is done on the selected data sets. The spectral analysis shows the evolution of wave spectra in space and time. In this way it is possible to relate variations in the spectra to differences in location in the measurement area and environmental conditions (see Figure 3-3).

To improve the reliability of the spectral analysis, the considered data series is divided in a number of blocks. All blocks individually serve as input for the wave spectrum. The use of more blocks improves the reliability. The downside of the use of more blocks is that it decreases the resolution of the wave spectrum. Influencing the resolution plays a large part in the considerations, since in the spectral analysis small data series are analysed. It is aimed for an optimum, considering both reliability and resolution, see Figure 4-13. The use of approximately 10 blocks is estimated to give a result that is both reliable and of good resolution, within the possibilities of this analysis.

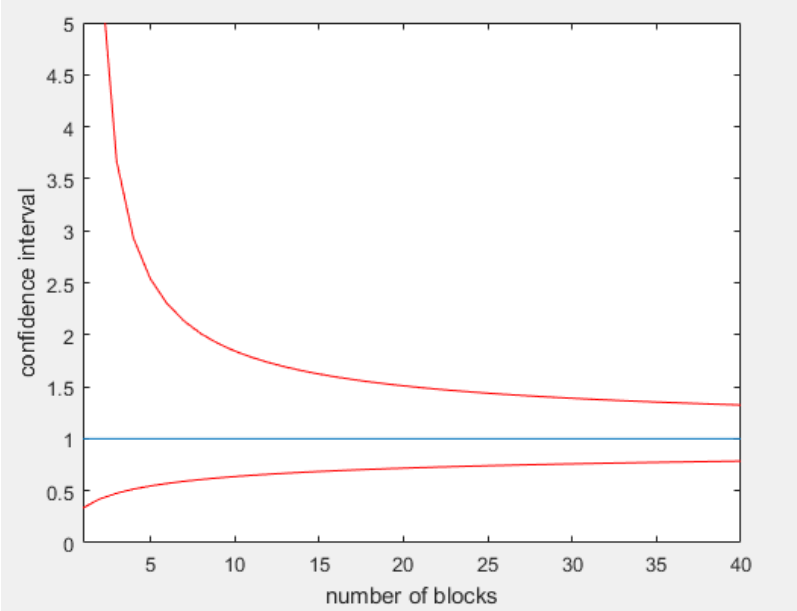

Figure 4-13. Confidence interval of a wave spectrum as function of the number of blocks in which the data series is divided

The first step in the spectral analysis is the analysis of temporal variations. The energy density spectrum of the 6 complete selected data sets is plotted in Figure 4-14. A distinction is made by colour between different grouped WRD deployments. Remember that the 1st, 2nd and 3rd deployment were during flood and the 4th, 5th and 6th during ebb. The figure shows clearly that during the measurement the wave conditions slowly change from rather uniform wave conditions with an energy peak at a frequency of approximately 0.16 Hz to non-uniform wave conditions. The energy spreads over different wave frequencies during the day, meaning that during the day the wave field gets more irregular. A possible explanation for this is the reversing tidal current, that gets more directly opposed to the wind direction during the day. Another possible explanation is the water level that decreases during the day (see Figure 3-3) inducing nonlinear shallow water wave effects to gain significance.

Further spectral analysis focuses on the spatial variation of the wave spectra. Wave spectra are generated for different moments of the deployments. These spectra, with their location indicated in a spatial plot, are all displayed in Appendix 0.

The plots in Appendix 0 do not show a clear relation between the location of the waves and the energy distribution of the waves. This implies that there is almost no variation of wave periods that can be ascribed to variations of the bathymetry.

The plots in Appendix 0 do show a correlation between the direction of the current and the distribution. All deployments during ebb, that is with waves and current in opposing direction, the peaks of the waves seem to be lower (all below 0.2 m^2/s) than the peaks of the spectra during flood. One deployment during flood (WD001_d2_s1), shows low energy peaks. This deployment was in a moment of the tidal wave close to high water slack, which explains the lower energy peaks. This observation corresponds with a previous observation from Figure 4-14. From the observation it can be concluded that when the current and the waves are aligned the waves become more uniform.

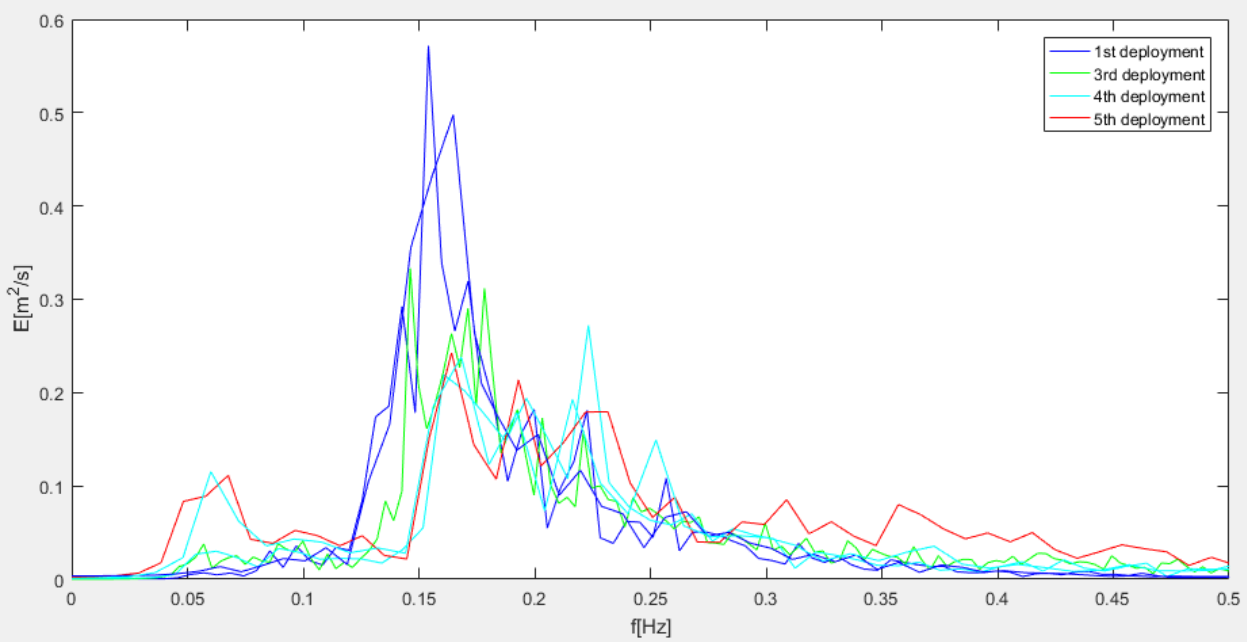

Figure 4-14. Wave spectra for vertical displacement, ordered by grouped WRD deployment

4.2.3. Comparing frames of reference

In this section the measurements in different frames of reference are compared. For this comparison the measurements from the WRD's and that of a fixed pressure sensor are used. Based on the previous analysis an expected difference is quantified in section 4.2.3.1. The actual comparison is made in section 4.2.3.2.

4.2.3.1. Theoretical Doppler shift

The difference between the position of the observer in a Eulerian and a Lagrangian frame of reference should, according to the theory on the Doppler shift (see sections 2.2 and 2.3), give differences in resulting wave data. This difference creates a discrepancy between the results of the WRD measurements and the prevailing knowledge on wave motions. After all, the prevailing knowledge is based on measurements from a fixed location. Therefor the influence of a Doppler shift on the wave measurements is investigated.

For application of Equation 1 the measured, relative frequency, the wave number of the wave and the current velocity are required. All these input variables are constantly changing over the duration of a deployment. For convenience a single constant value is used for the investigation of the Doppler-shift. Note that, because of these assumptions, the result is just an indication for an order of magnitude of the occurring Doppler shift.

The current velocity U_n is gained from another part of the research associated to the *Drifters in SEAWAD Field campaign*. According to this research by Thomas Vos the magnitude of the tidal current during the measurements on the 9th of September varied from 0.3 m/s till 1.4 m/s. The largest value is hold normative, since this gives the largest Doppler shift. If this largest Doppler shift is calculated, it is known what can be expected in terms of frequency shift by the Doppler-effect.

Wave number k is gained by applying the dispersion relation (Equation 5). For the application of this formula the water depth is approached again by 7 m. The used frequency is 0.15 Hz since this is a value at or close to which the most energy density spectra have a peak, it is the mode of the data set. Application of these values in the dispersion relation results in a wave number k = $1.55*10^{-2}$ rad/m.

Applying U_n = 1.4 m/s and k = $1.82*10^{-2}$ rad/m gives a Doppler shift of 0.022 Hz. Although this shift is not negligible, it is also not really significant in this research. The large number of processes that play a part in the coastal system and the variability of each of them, does make one of them individually hardly observable. Note that for larger frequencies the wave number and with that the Doppler shift gets larger and vice versa. It is observed that approximately 0.05 Hz and 0.40 Hz are the lower and upper limit of the observed wave frequencies. For these values, as well as for the observed peak frequency of 0.15 Hz, the expected Doppler shift is calculated and displayed in Table 4-3.

Table 4-3. Expected Doppler shifts for different values of the wave frequency.

	ω [rad/s]	k [rad/m]	Expected Doppler shift [Hz]
Lower limit	0.05	$5.16 * 10^{-3}$	0.007
Conditions	0.15	$1.55 * 10^{-2}$	0.022
Upper limit	0.40	$4.18 * 10^{-2}$	0.059

4.2.3.2. Measurements of different frames of reference

On theoretical grounds a Doppler shift is present between the measurements in different frames of reference. A comparison between these measurements is made to make visible what the effect is of a Doppler shift on the comparability between the WRD measurements and the pressure sensor measurements.

In Figure 4-8 it is shown that the drifters pass by some of the fixed measurement frames and pressure sensors. The data of the fixed measurement frames was unavailable at the moment of this research. The data of the pressure sensors was available. Figure 3-2 shows that pressure sensors I and K where the sensors that were passed by on shortest distance. From these pressure sensors, sensor I has failed doing correct measurements, meaning that only the data of pressure sensor K can be used. Two WRDs passed close by this sensor: WD001_d2_s1 and WD001_d4_s0. These trajectories are used for comparison with the data of pressure sensor K.

For a good comparison, the compared data sets must represent equal information. The data of the pressure sensor gives the evolution of the water pressure in time, at a certain height in the water. By converting the pressure to the amount of water above the sensor, the surface elevation is obtained. By means of a filter on the frequencies of harmonic components of the waves, data with the wave motions between 0.05 and 1.0 Hz only is gained. This is a processing step like the one elaborated on in section 4.1.1.2. After this step the data is suitable for comparison.

To make a good comparison with the wave spectra from the WRD measurements, the wave spectra from the pressure sensor measurements are drafted in the same way (see section 4.2.2). This means that the spectrum is for an equal time bin and with an equal resolution. The points of closest passage of WD001_d2_s1 and WD001_d4_s0 are that of spectrum 7 and spectrum 2 respectively. The spectra and the location they apply to are shown in Appendix 0. These spectra are the spectra that are compared with spectra from the pressure sensor. The comparison is displayed in Figure 4-15.

Figure 4-15 shows that the compared spectra show large similarities. First of all the distribution of the energy over the spectrum, e.g. the location of energy peaks and the bin that contains the bulk of the energy, looks very similar. Also the magnitude of the energy density on certain frequencies in the compared spectra is much alike. The large similarity matches previous calculations.

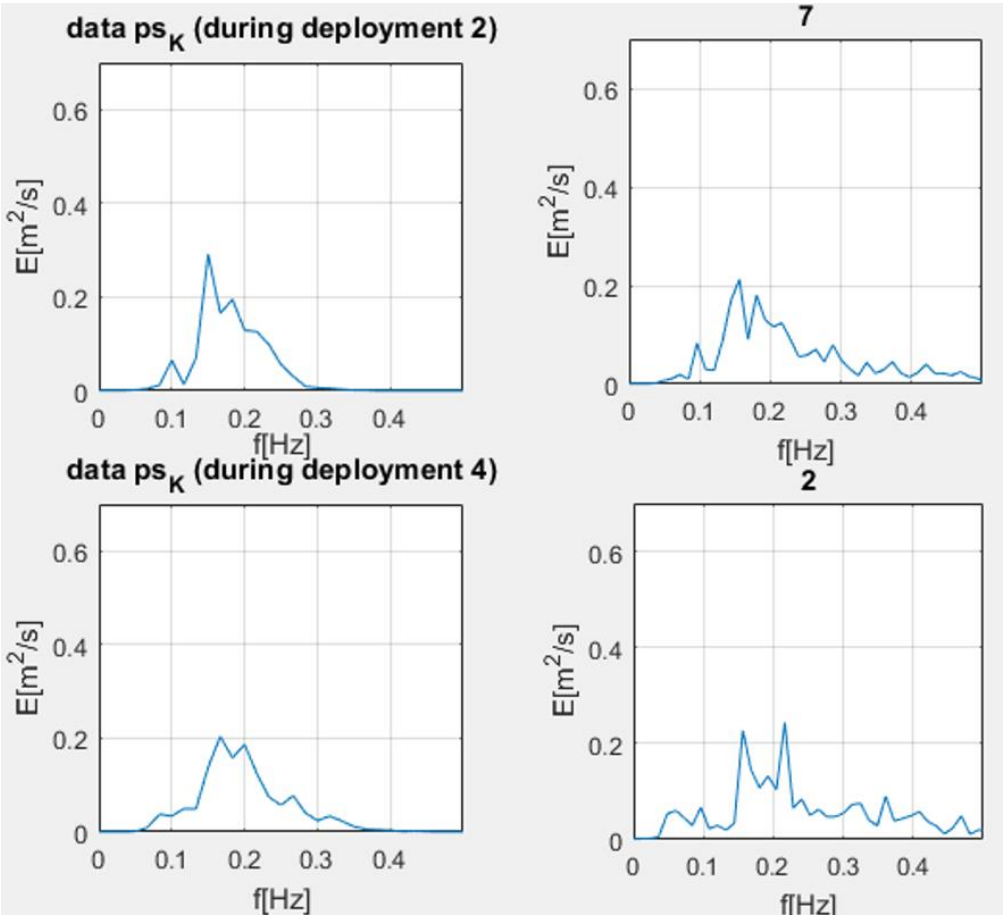

Figure 4-15. A comparison between the wave spectra obtained from measurements in a Eulerian frame of reference (left) and in a bypassing Lagrangian frame of reference.

Besides similarities, also differences exist between the compared spectra, that could be explained by the small spatial difference of measurement location and the non-uniform Doppler-shift. The latter explanation is the phenomenon that the magnitude of a Doppler-shift depends on the wave length (wave number k) and on the angle between the current and the waves by U_n. Different wave components can be of different wave lengths. They also can travel in different directions thus have a different U_n. This means that a Doppler-shift can be different for each harmonic component. Although the overall effect of the Doppler-shift seems to be small, this difference in effect can cause deformation of the spectrum.

Based on this investigation it can be concluded that measurements results from a WaveDroid (Lagrangian frame of reference) and a pressure sensor (Eulerian frame of reference) give similar results. The Doppler shift is not of a significant influence on the wave data. WaveDroids are suitable for measuring the bulk of the wave energy, the frequency range of the wave field and the rough outline of an energy density spectrum. Overall it can be concluded that it is possible to compare wave spectra that are measured in a Eulerian and in a Lagrangian frame of reference without the need to do data converting computations. The WaveDroid, applied as a WRD, is suitable for doing wave measurements.

5. Conclusions

This section contains the conclusions of this research. These conclusions are only the preliminary conclusions on this subject. The issues in the knowledge and this research that are open for discussion are also pointed out. From this discussion, recommendations for a future research trajectory are drawn.

5.1. Conclusions

The use of WRDs to measure the wave field has the large advantage that one device measures both changes in time and in space. A drawback of using WRDs is that, because of the fact that the measurement device moves, more measurement errors enter the measured data. The errors can best be observed in the presence of energy in the low frequency region of the spectrum and in the presence of statistical unlikely large waves. The errors can largely be removed by filtering on harmonic wave components of certain frequencies and by removing the data in certain time frames.

The Doppler shift between the measurements in different frames of reference has been investigated. From this investigation it is concluded that a Doppler shift is present but is usually very small and of no significant influence on the wave signal. Only for very short wave components and in the presence of a strong current velocity the influence becomes significant.

The spectral analysis and wave-by-wave analysis of data measured by a WaveDroid gives and of the data measured by a fixed pressure sensor give comparable results. Data from wave measurements by WRD's can be directly compared to data from wave measurements by fixed devices. It is concluded that WaveDroid measurements are useful in wave measurements and analysis.

In the interpretation and analysis of the data no coastal process is observed to be clearly prevailing over others. This lack of evidence for the presence of a specific process implies that the coastal area of the ebb tidal delta is very complex and contains very much processes that are of importance. This implication is matching the expectations. Besides emphasizing the complexity of the coastal dynamics, no conclusion can be drawn on the coastal dynamics.

5.2. Discussions

The flawed raw data is during processing corrected. The data that is judged to be correct and suitable for analysis is used. This judgment is based on the fact that no errors were observed anymore. The processing steps of filtering the data of certain time frames and filtering of harmonic components has deformed the data. It is possible that the processing steps have harmed the relation between the wave field that is experienced by the WRD and the wave field that is shown by the corrected data and it is also possible that these errors are not clearly observable.

During processing the data on horizontal wave motion is filtered out. It is decided to do so because the wave data on horizontal motions did not fit the expected wave height distribution. The knowledge on wave height distribution is gained from research on vertical motions (it is expected to be Rayleigh distributed). This knowledge is applied on the horizontal motions as well, resulting in time series with many wave heights that are judged to be errors. The validity of the application of the knowledge on vertical wave height distribution on the horizontal motion is uncertain.

5.3. Recommendations

Based on the conclusions and points of discussions the following continuations of this research are recommended:

- More research on the correctness of the wave data that results from processing and correcting. As mentioned it is possible that the waves shown by the data deviate from the experienced waves at sea. If this is the case at least the effect of this deviation must be known. Ideally, once the error is known, it can be removed.
- More research on the representation of the horizontal wave motion. This research is twofold. On the one hand, it must be investigated what the expected wave field representations, like wave height distribution, of the horizontal wave motion are. On the other hand it must be investigated what corrective processing steps are required to make the wave data fit the expected wave field representations.
- More research on the validity of the comparison of the measurements in different frames of reference. It is concluded that data from wave measurements in different frames of reference can be directly compared to one another. This conclusion however is drawn based on a comparison of a large part of the wave field. Nothing can be concluded yet about the validity of that comparison if only a particular detail of the wave data is compared. For instance if only waves from a certain direction is compared. More research on this subject leads to the insight of the validity of the comparison between the different frames of reference, on the level of individual processes.
- Further analysis and interpretation of the measurement data. For this research not all data sets are interpreted. Furthermore, there are methods for analysis that are not applied yet. For instance, 2D spectral analysis is not applied. A more extensive analysis and interpretation of the wave data can lead to a better insight in the processes that play a part in the coastal dynamics of the Wadden Sea tidal inlet.

References

Battjes, J. A. & Groenendijk, H. W., 2000. Wave height distributions on shallow foreshores. *Coastal Engineering,* Volume 40, pp. 161-182.

Bosboom, J. & Stive, M. J. F., 2012. *Coastal Dynamics I.* 0.3 red. Delft: VSSD.

Briggs, M. J., Demirbilek, Z. & Green, D. R., 1996. Wave-Current Interaction in Inlets. *Coastal Engineering,* pp. 1219 - 1232.

Duran-Matute, D. et al., 2014. *A fresh look into transports in the Dutch Wadden Sea: results from 3D simulations.* Leeuwarden, 13th Symposium Waddenacademie.

Elias, E. P. L., Van der Spek, A. J. F., Wang, Z. B. & De Ronde, J. G., 2012. Morphodynamic development and sediment budget of the Dutch Wadden Sea over the last century. *Netherlands Journal of Geosciences — Geologie en Mijnbouw,* 91(3), pp. 293-310.

Herbers, T. H. C. et al., 2012. Observing Ocean Surface Waves with GPS-Tracked Buoys. *Journal of Atmospheric and Oceanic Technology,* pp. 944-959.

Hinkel, J. et al., 2013. A global analysis of erosion of sandy beaches and sea-level rise: An application of DIVA. *Global and Planetary Change,* Volume 111, pp. 150-158.

Holthuijsen, L. H., 2007. *Waves in Oceanic and Coastal Waters.* New York: Cambridge University Press.

Lai, R. J., Long, S. R. & Huang, E. H., 1989. Laboratory Studies of Wave-Current Interaction: Kinematics of the Strong Interaction. *Journal of Geophisical Research,* pp. 201-214.

Michel, T., Fourati, H., Geneves, P. & Layaida, N., 2015. *A Comparative Analysis of Attitude Estimation for Pedestrian Navigation with Smartphones.* Banff (Canada), 2015 International Conference on Indoor Positioning and Indoor Navigation.

Munk, W. H., 1950. *Origin and Generation of Waves - Proceedings of First Conference on Coastal Engineering.* Long Beach, Council on Wave Research.

Oost, A. P., Wang, Z. B., De Groot, A. V. & Van der Valk, L., 2014. *Preparing for climate change: an adaptive strategy for Wadden Sea Area,* Delft: Deltares Report 1209152.

Peregrine, D. H. & Jonsson, I. G., 1983. *Interaction of Waves and Currents,* Fort Belvoir: U.S. Army, Corps of Engineers, Coastal Engineering Research Center.

Rijkswaterstaat, 2017. *Rijkswaterstaat Waterdata.* [Online]
Available at: https://www.rijkswaterstaat.nl/water/waterdata-en-waterberichtgeving/waterdata
[Geopend 15 september 2017].

Ruessing, B., Ramaekers, G. & Van Rijn, L. C., 2012. On the parameterization of the free stream non-linear wave orbital motion in nearshore morphodynamic models. *Coastal engineering,* Volume 65, pp. 56-63.

Stive, M. J. F. et al., 2013. A New Alternative to Saving Our Beaches from Sea-Level Rise: The Sand Engine. *Journal of Coastal Research,* 29(5), pp. 1001-1008.

Wavedroid, 2017. *Datasheet Revision 1.* [Online]
Available at: http://www.wavedroid.net/files/WaveDroid_datasheet_block2.pdf

Figures

Figure 2-1. The Composite Weibull distribution (Holthuijsen, 2007) 7
Figure 3-1. Location of measurement devices SEAWAD in the Amelander Zeegat (Courtesy of S.G. Pearson, 2017) 11
Figure 3-2. WRD deployment area with measurement devices (Courtesy of S.G. Pearson, 2017) 11
Figure 3-3. Water level at Terschelling Noordzee (left), wave height at Schiermonnikoog Westgat Buiten (middle), wind speed and wind direction at Terschelling Noordzee (both right) as observed during deployment (Rijkswaterstaat, 2017) 12
Figure 3-4. WaveDroid, typical deployed configuration (Wavedroid, 2017) 13
Figure 4-1. WRD trajectories (red lines) with indication on starting position of data set (green dots), locations of the measurement frames (black circles) and the locations of the pressure sensors (yellow dots), on 9 September 2017 between 9:00 and 17:00 h. The bottom level is shown by the coloured scale. 15
Figure 4-2. Displacement spectra resulting from conventional (default) processing order and the delayed magnetic correction (WD001 d5 s0). Both spectra of horizontal motions are influenced in different amounts, the spectrum of vertical motion is not influenced. 19
Figure 4-3. An arbitrary Rayleigh distribution with $H_{99.9\%}$ and $H_{1/3}$ indicated 21
Figure 4-4. Application of a Rayleigh based filter on the ends of the data series on the wave height, with in red indicated the threshold wave height (WD001_d4_s0). 22
Figure 4-5. The effect of the filtering of large waves at the start and end of the data. The left plots display the time series and the right plots display the energy spectra (WD001_d4_s0). 22
Figure 4-6. The normalized occurrence of wave heights in a deployment compared with the best fitting Rayleigh distribution for a data set of which the ends are not filtered (top three plots) and the ends are filtered (bottom three plots). 23
Figure 4-7. Energy density spectra after processing. Left a spectrum still containing low frequency energy (WD001_d4_s1) and right a spectrum cleaned from low frequency energy (WD002_d1_s0). 24
Figure 4-8. Trajectories of the selected WRD deployments (red) with indication on starting position of data set (green), locations of the measurement frames (black circles) and the locations of the pressure sensors (yellow). 25
Figure 4-9. Temporal evolution of the wave height (top plot) and the wave period (bottom plot). Each deployment is shown in a different color and the trends per deployment are indicated by black lines. 26
Figure 4-10. Trend lines of the temporal evolution of the wave height (top plot) and the wave period (bottom plot). Colours are matching the colours in Figure 4-9. 26
Figure 4-11. Trend lines of the temporal evolution of the wave height (top plot) and the wave period (bottom plot), zoomed in on deployment 3. 27
Figure 4-12. Evolution of the significant wave height of two different deployments, the top one during flood (WD001_do_s0) and the bottom one during ebb (WD001_d4_s0). 28
Figure 4-13. Confidence interval of a wave spectrum as function of the number of blocks in which the data series is divided 29
Figure 4-14. Wave spectra for vertical displacement, ordered by grouped WRD deployment 30
Figure 4-15. A comparison between the wave spectra obtained from measurements in a Eulerian frame of reference (left) and in a bypassing Lagrangian frame of reference. 32

Tables

Table 3-1. Conditions during WRD deployments, between 09:00 and 17:00 9 September 2017 (Rijkswaterstaat, 2017)....12
Table 3-2. Deployment times sorted by grouped WDR deployment....13
Table 4-1. Overview of data series with their names and covered length in time ordered by WaveDroid and deployment, with the data series that are judged to be too short marked in grey.17
Table 4-2. Overview of the data series selected for further analysis....24
Table 4-3. Expected Doppler shifts for different values of the wave frequency. 31

Appendix

A. Data management

A.1.

Data removal during processing

This appendix shows an overview of the data throughout the processing. The processing steps are displayed in chronological order. The data files that are listed are the data files that exist after the application of the time step correction (see section 0). In this process step some of the raw data files are split. The lengths of the data files, both in time and in data points, is the length at the start of the processing. The length of some data files is adjusted in the processing.

The following processing steps are applied:

- **Removed for insufficient length**: Data files that are too short give unreliable results and not representative information. The data files that are shorter than 10 minutes are removed from further analysis (see section 0).

- **Removed for too much large waves**: Parts of data files that contain too much too large waves are cut away in the processing. Some data files contain so much waves of too large height and/or contain them scattered in time that after cutting erroneous parts no data of useful length is left. These data files are therewith removed from further analysis (see section 4.1.2.2).

- **Removed for lasting low freq. energy**: After correcting observed errors by deleting known causes, some data still contains erroneous low frequency energy. These data sets are judged to be not reliable. Therefor they are deleted from further analysis and interpretation (see section 4.1.2.3).

- **Removed from final selection**: For the interpretation of the wave data a selection of the available data is made. This selection is based on the wave height distributions and the energy density spectra of the measured data. In this selection some data files are removed from further analysis and interpretation (see section 4.1.2.3.).

Deployments [-]	Δt [min:s]	n_{data} [-]	Processing steps				
			Removed for insufficient length	Removed for too much large waves	Removed for lasting low freq. energy	Removed from final selection	Interpreted data
WD001_d0_s0	30:00	9000					O
WD001_d1_s0	03:15	977	X				
WD001_d1_s1	26:41	8605				X	
WD001_d1_s2	03:01	909	X				
WD001_d2_s0	01:02	310	X				
WD001_d2_s1	47:56	14384					O
WD001_d3_s0	20:00	6000					O
WD001_d4_s0	24:35	7376					O
WD001_d4_s1	20:24	6122			X		
WD001_d5_s0	35:00	10500		X			
WD002_d0_s0	30:00	9000				X	
WD002_d1_s0	35:00	10500				X	
WD002_d2_s0	49:00	14700		X			
WD002_d3_s0	20:00	6000				X	
WD002_d4_s0	45:00	13500			X		
WD002_d5_s0	35:00	10500			X		
WD003_d0_s0	30:00	9000					O
WD003_d1_s0	28:16	8480				X	
WD003_d1_s1	06:42	2013	X				
WD003_d2_s0	49:00	14700				X	
WD003_d3_s0	13:57	4186					O
WD003_d3_s1	06:02	1812	X				
WD003_d4_s0	00:57	286	X				
WD003_d4_s1	36:59	11099			X		
WD003_d4_s2	07:02	2111	X				
WD003_d5_s0	35:00	10500			X		

A.2.
Observed erroneous wave signals

The table in this appendix indicates for the data on wave motions for three directions, whether or not it contains erroneous wave signals.

The observation of errors diverge in clarity of the error. Some of the errors show magnitudes of waves in the signal are clearly not realistic but some magnitudes of waves might be realistic. In some wave signals the number of waves that are typed as erroneous is that large that there is clearly an error but in some wave signals that number is limited, questioning the existence of an error.

Besides judging the presence of large waves the presence of a disproportional amount of low frequency energy is judged to determine whether or not a data set contains errors.

Deployments [-]	Data containing errors		
	Vertical motion	Northward motion	Westward motion
WD001_d0_s0			X
WD001_d1_s1	X	X	X
WD001_d2_s1		X	X
WD001_d3_s0		X	X
WD001_d4_s0	X	X	X
WD001_d4_s1	X	X	X
WD001_d5_s0	X	X	X
WD002_d0_s0		X	
WD002_d1_s0	X	X	X
WD002_d2_s0	X	X	X
WD002_d3_s0	X	X	X
WD002_d4_s0	X	X	X
WD002_d5_s0	X	X	X
WD003_d0_s0			X
WD003_d1_s0	X	X	X
WD003_d2_s0		X	X
WD003_d3_s0		X	X
WD003_d4_s1	X	X	X
WD003_d5_s0	X	X	X

A.3.
Wave removal from deployments

The table in this appendix gives an overview of the data sets that are filtered on the erroneous signals in the vertical wave motion. This erroneous behavior is observed in the wave heights, wave periods and wave energy spectra.

A removal of observed large waves is done. The table gives per deployment the string of waves that is remained after the removal. The selection mentions the wave numbers in the unfiltered (on large waves at the ends) data. After the manual selection the remaining data is filtered on large waves at the ends.

The length of the removed strings depends on the length of the error and length of the remaining data sets. If the remaining data set is short it is directly removed as well, like in section 0.

Note that two data sets are entirely removed. This is because the errors were present scattered throughout the data, resulting in too short error-free data strings. This reduces the total number of data series to 17.

Deployments	Waves remaining based on exceeding wave height and period		n_{data}	length
[-]			[-]	[min]
WD001_d0_s0	1 - 371	(till end)	8778	29:15
WD001_d1_s1	1 – 246		5351	17:50
WD001_d2_s1	1 - 727	(till end)	14026	46:45
WD001_d3_s0	1 - 321	(till end)	5618	18:43
WD001_d4_s0	112 - 421	(till end)	5185	17:17
WD001_d4_s1	1 - 223		4111	13:42
WD001_d5_s0	-		-	-
WD002_d0_s0	1 - 216		5650	18:50
WD002_d1_s0	185 - 488	(till end)	6364	21:12
WD002_d2_s0	-		-	-
WD002_d3_s0	117 - 297	(till end)	3508	11:41
WD002_d4_s0	1 - 555		10526	35:05
WD002_d5_s0	130 - 555	(till end)	8027	26:45
WD003_d0_s0	141 - 360	(till end)	5477	18:15
WD003_d1_s0	229 - 375	(till end)	3284	10:56
WD003_d2_s0	228 - 652		8190	27:18
WD003_d3_s0	1 - 228	(till end)	4162	13:52
WD003_d4_s1	184 - 637	(till end)	7961	26:32
WD003_d5_s0	1 - 319		5586	18:37

B. Variances

The table in this appendix shows the variances of displacement of the low frequency waves (f < 1.0 Hz) for two orders of processing; the default order and the changed order in which the magnetic correction is delayed. Further it shows the variance after filtering the erroneous starts and ends of the data series.

The variance is a measure for the existence of wave energy in the low frequency regions of the spectrum. The physical meaning of the variance is vague in this context. The use of the variance is therefore not to quantify some physical itself but to express the magnitude of the improvement made by processing. One must not look at the value of the variance of one moment in the process for one deployment, but to the change in variance throughout the process.

The green cells indicate the deployments that significantly improved compared with the previous cell. The red cells indicate the deployments that significantly deteriorated compared with the previous cell.

Deployment	Variance northward displacement			Variance westward displacement		
[-]	Default order [m]	Changed order [m]	Start, end filtered [m]	Default order [m]	Changed order [m]	Start, end filtered [m]
WD001_d0_s0	0.0081	0.0083	0.0083	0.0071	0.0075	0.0075
WD001_d1_s1	0.0757	0.0966	0.0261	0.0783	0.0179	0.0152
WD001_d2_s1	0.0523	0.0300	0.0303	0.0572	0.0406	0.0243
WD001_d3_s0	0.1101	0.1128	0.0594	0.0726	0.0527	0.0214
WD001_d4_s0	0.3357	0.5366	0.0742	0.2808	0.2430	0.0690
WD001_d4_s1	0.4145	0.1034	0.0880	0.2600	0.1095	0.0886
WD001_d5_s0	0.1642	0.1578	0.0863	0.6268	0.2043	0.0817
WD002_d0_s0	0.1123	0.0181	0.0112	0.1636	0.0089	0.0066
WD002_d1_s0	0.1756	0.1009	0.0361	6.7046	0.2402	0.0353
WD002_d2_s0	0.4127	0.0489	0.0417	0.3087	0.0341	0.0308
WD002_d3_s0	2.7040	0.0775	0.0528	0.3418	0.0842	0.0485
WD002_d4_s0	0.3193	0.4500	0.3286	0.4724	0.5611	0.1402
WD002_d5_s0	2.4387	0.8672	0.5779	0.7600	1.2101	0.4230
WD003_d0_s0	0.0108	0.0109	0.0055	0.0068	0.0068	0.0066
WD003_d1_s0	0.2044	0.2038	0.0335	0.0330	0.0329	0.0310
WD003_d2_s0	0.0321	0.0321	0.0255	0.0532	0.0532	0.0307
WD003_d3_s0	0.0503	0.0500	0.0433	0.1483	0.1487	0.0541
WD003_d4_s1	0.3609	0.3583	0.2039	1.6103	1.6123	0.1543
WD003_d5_s0	0.3964	0.3968	0.0763	0.6803	0.6746	0.0743

C. Remaining data for analysis

This appendix shows the data series of the deployments that are selected for analysis and interpretation after processing. This appendix shows for all the remaining data the wave height distribution with the best fitting Rayleigh distribution, the energy density spectrum, the surface elevation in time and the wave height in time. Note that the considered data series at this point only consist of representation of vertical motion. From the data series remaining at this point, a selection can be made for further analysis of the wave field.

WD001_d0_s0

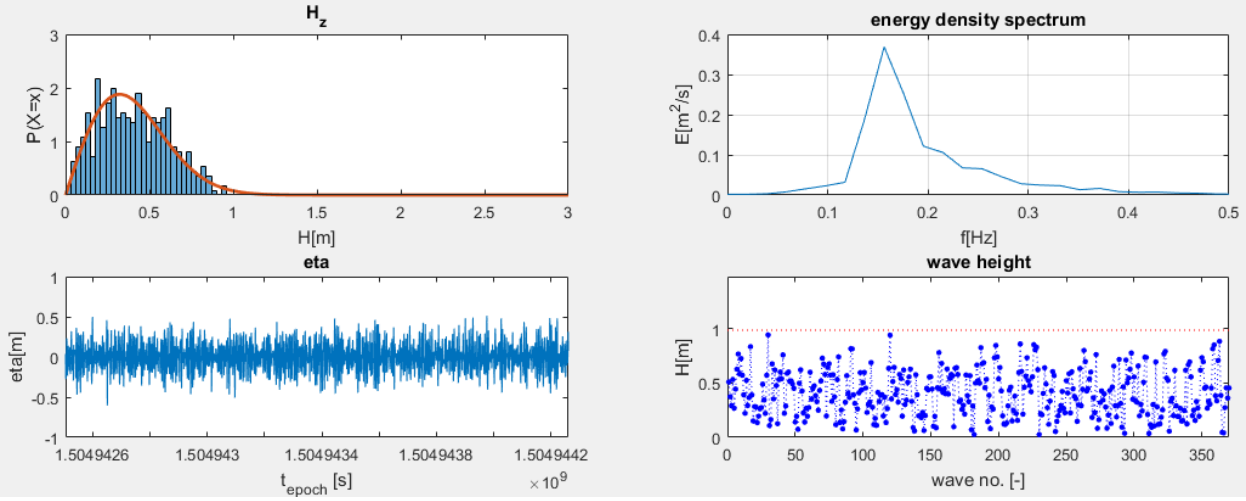

WD001_d2_s1

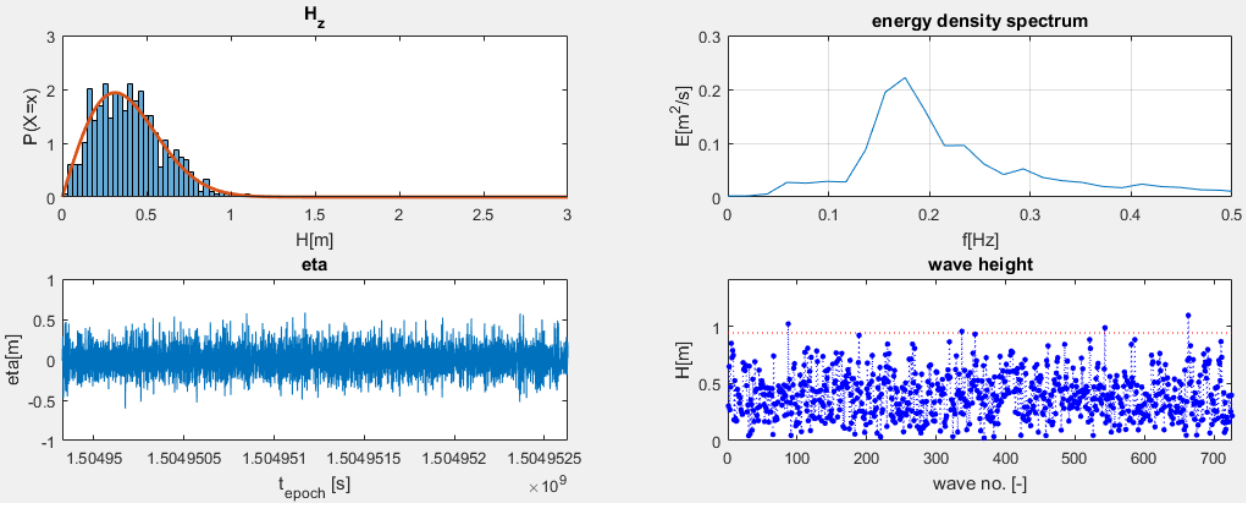

WD001_d3_s0

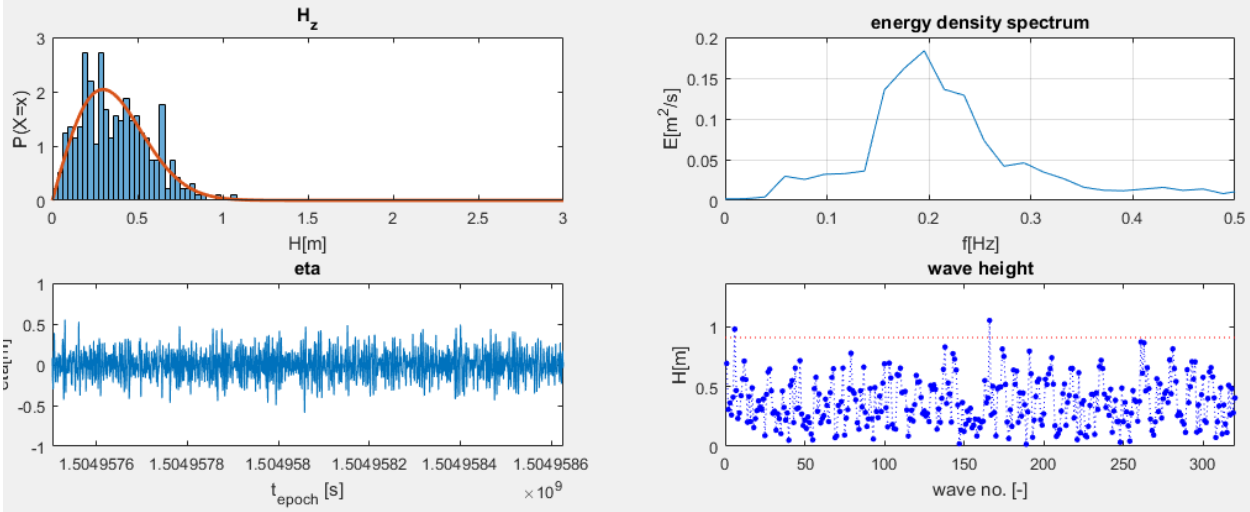

WD001_d4_s0

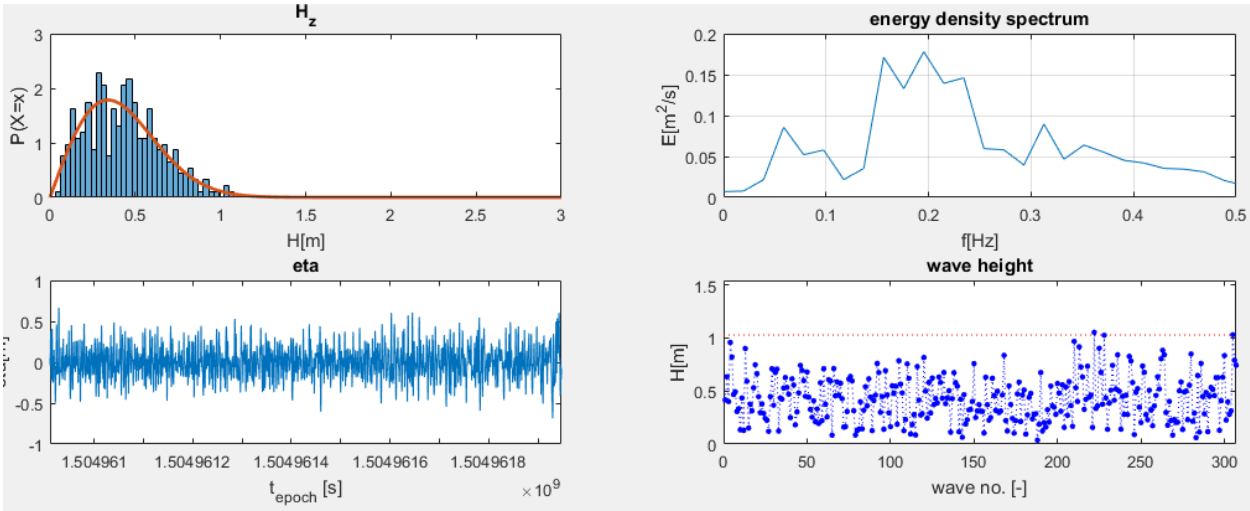

WD003_d0_s0

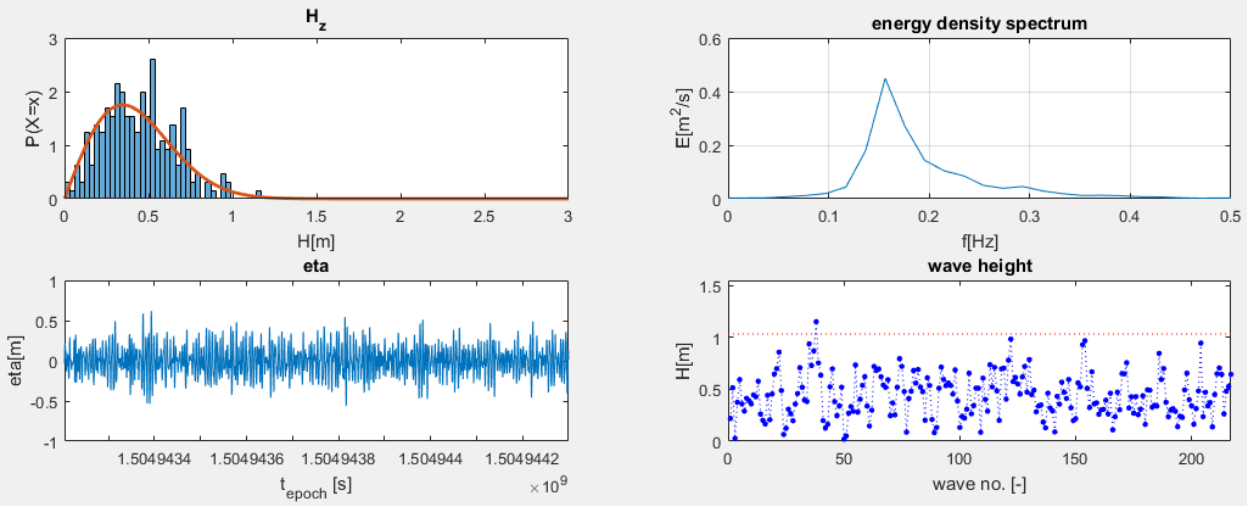

WD003_d3_s0

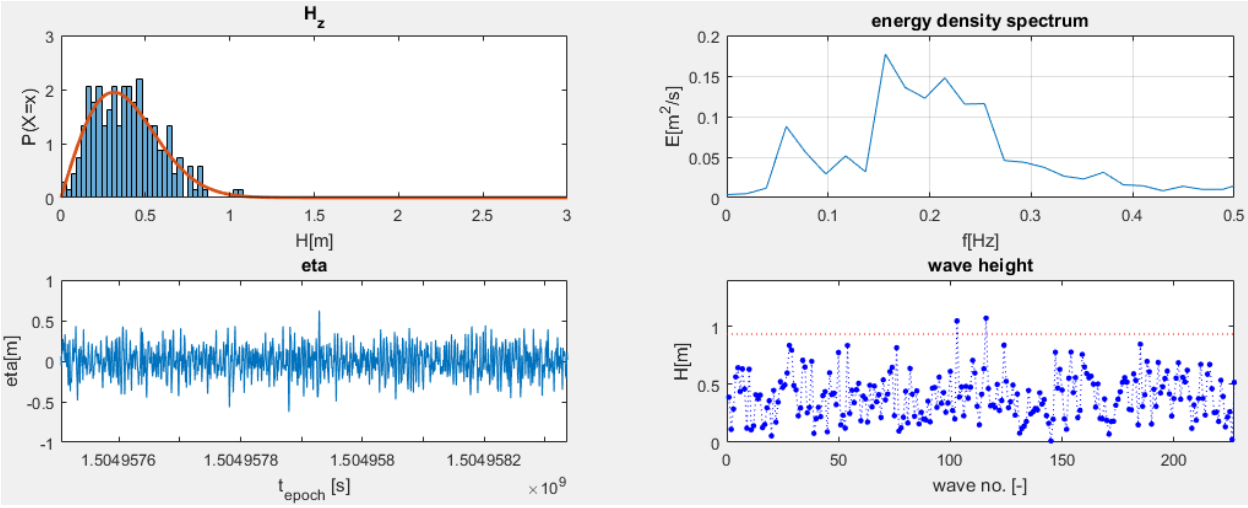

D. All results wave-by-wave analysis

This appendix shows the results of analysis of the spatial variation of wave characteristics that follow from the wave by wave analysis. The figures below show the WRD trajectory with the significant wave height, obtained from wave by wave analysis

The figures must be read as follows. The significant wave height represents the waves for a data string covering 10 minutes of deployment. Significant wave heights are calculated for time slots of 5 minutes with an interval of 2 minutes to show the evolution of the spectrum.

WD001_d0_s0 flood

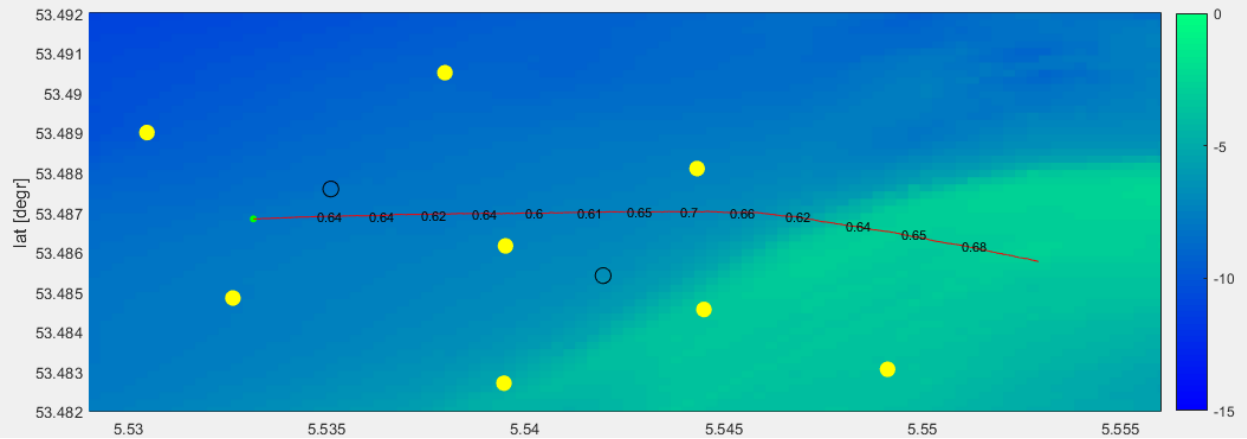

WD001_d2_s1 flood

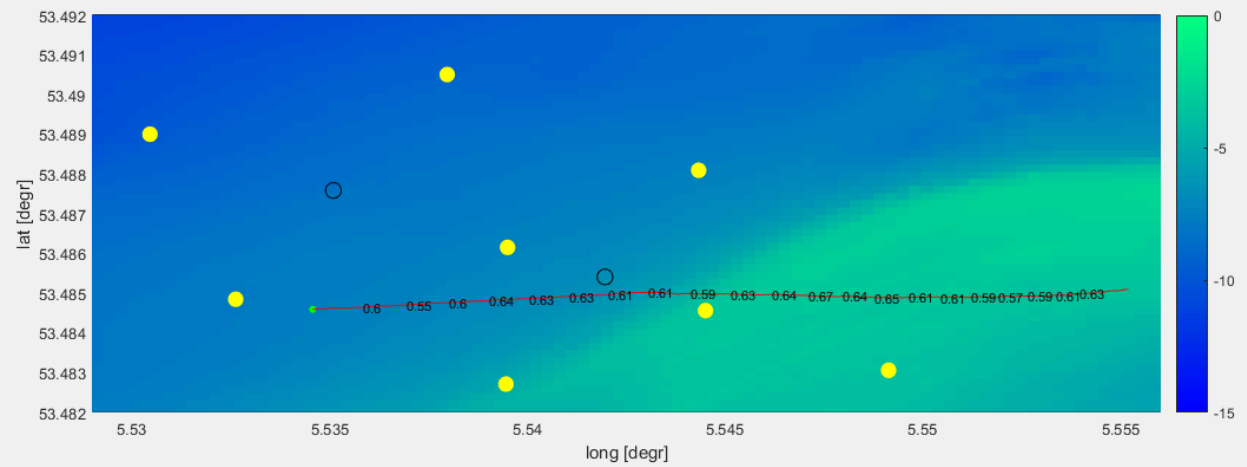

WD001_d3_s0 ebb

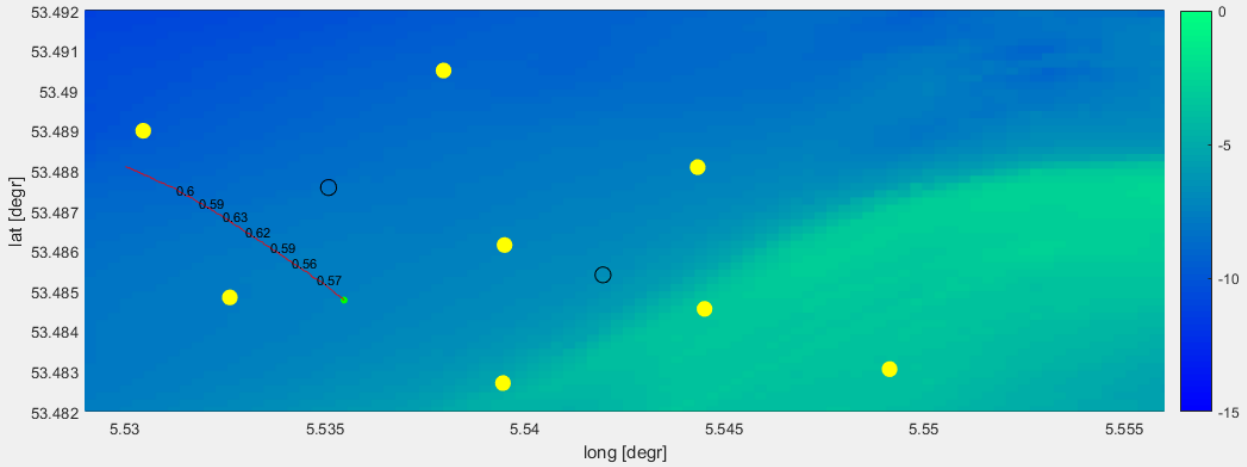

WD001_d4_s0 ebb

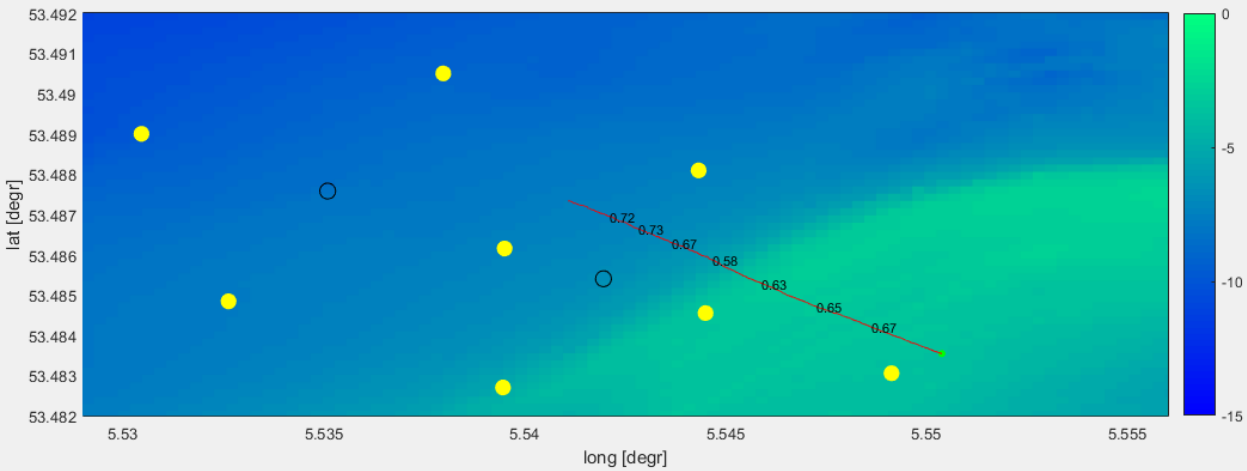

WD003_d0_s0 flood

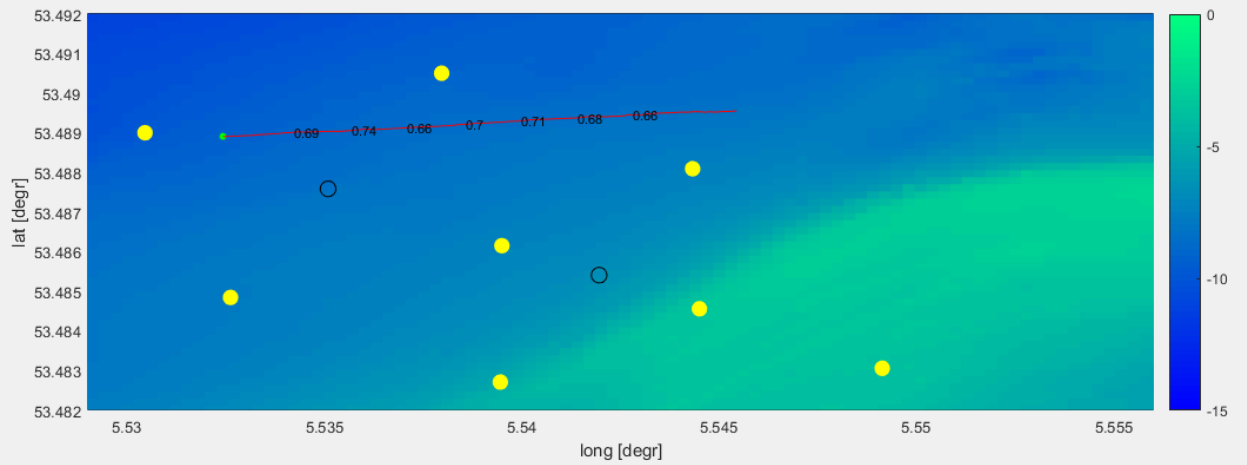

WD003_d3_s0 ebb

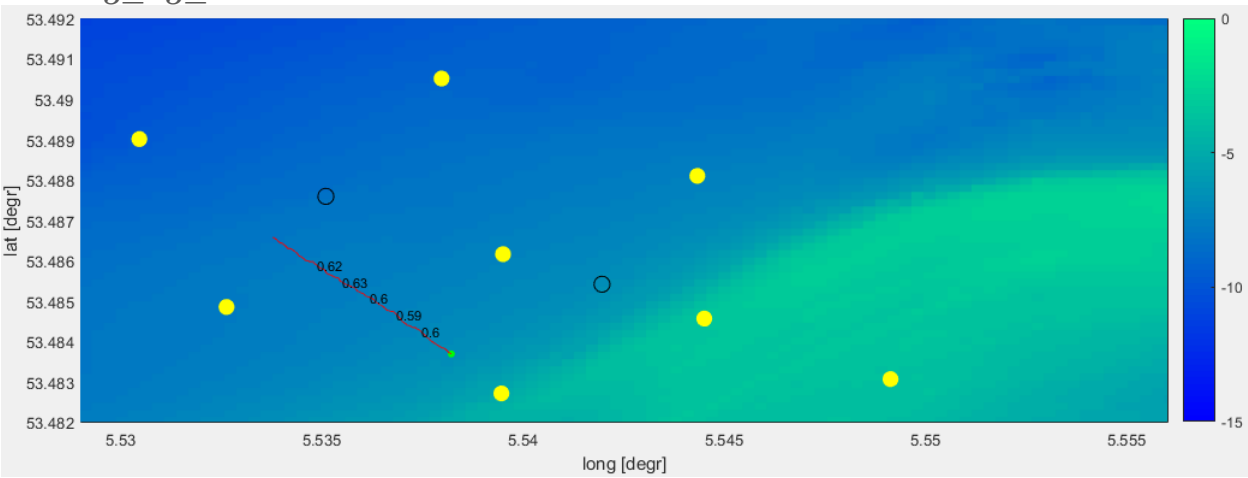

E. All results spectral analysis

This appendix shows the results of analysis of the spatial variation of the energy density spectra. The figures below show the WRD trajectory with the accompanying spectra.

The figures must be read as follows. Each spectrum is an energy density spectrum for a data string covering 10 minutes of deployment. The number, belonging to the spectrum, is displayed in the spatial plot at the position where the WRD was halfway the deployment. Spectra are drafted for time slots of 10 minutes with an interval of 2.5 minutes to show the evolution of the spectrum.

WD001_do_so flood

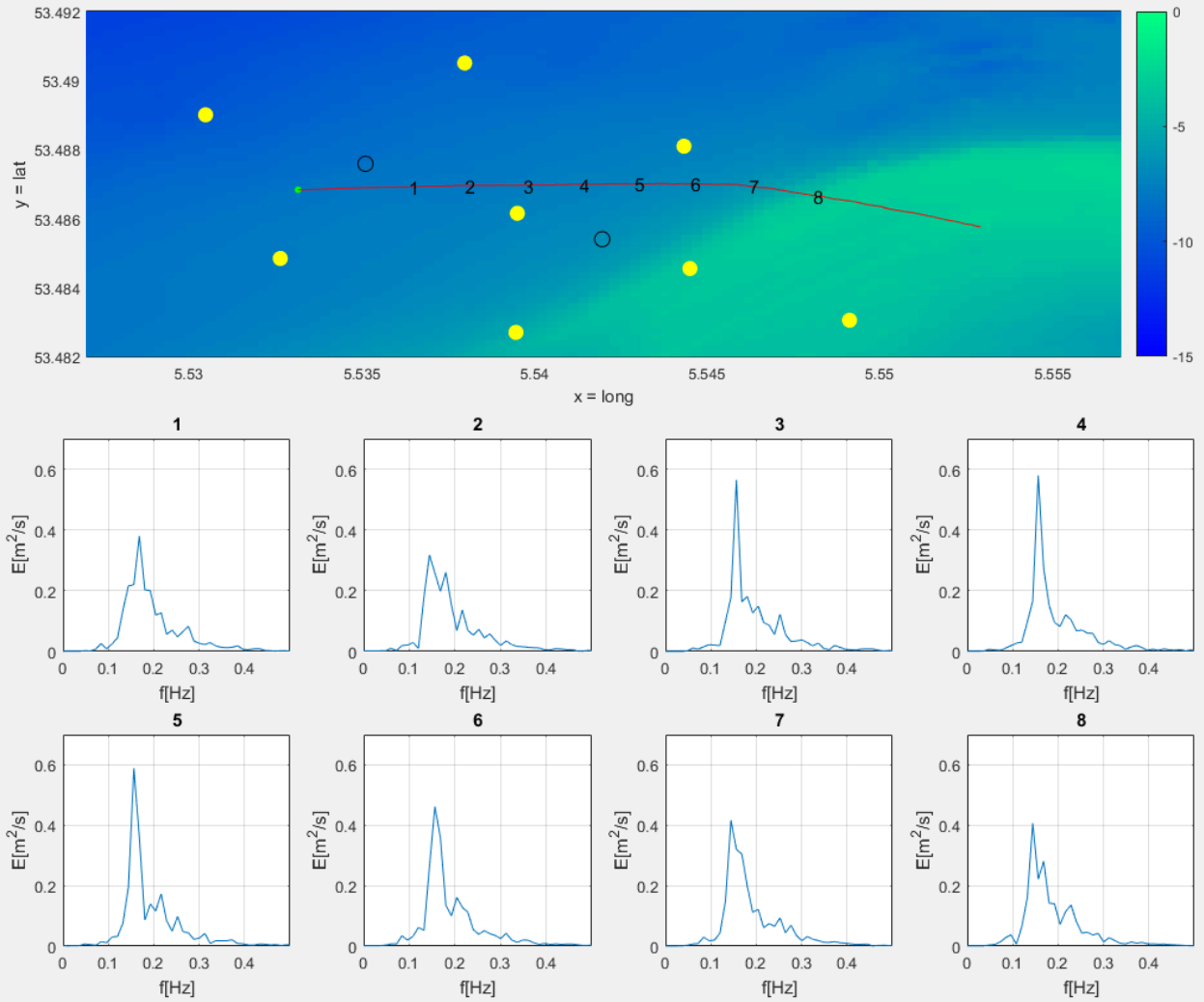

WD001_d2_s1 flood

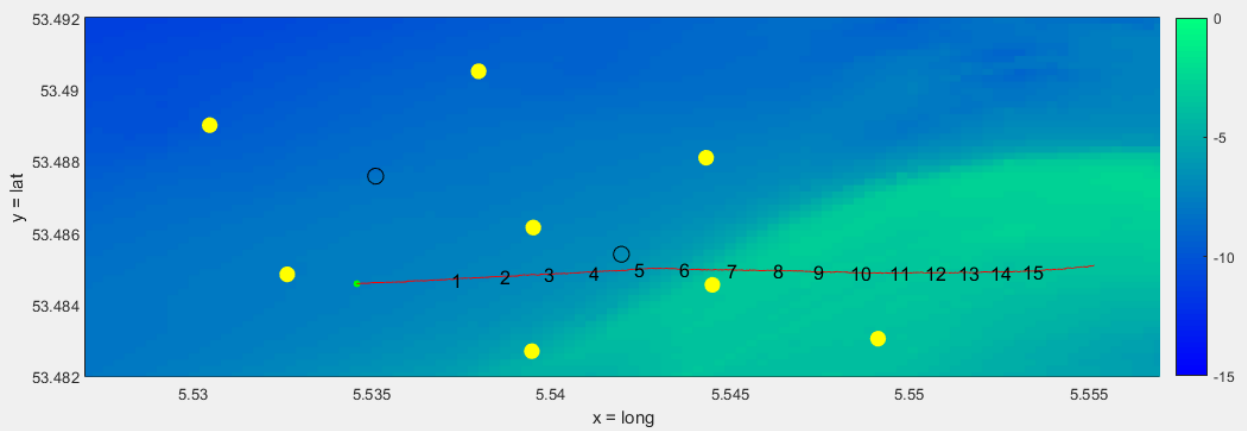

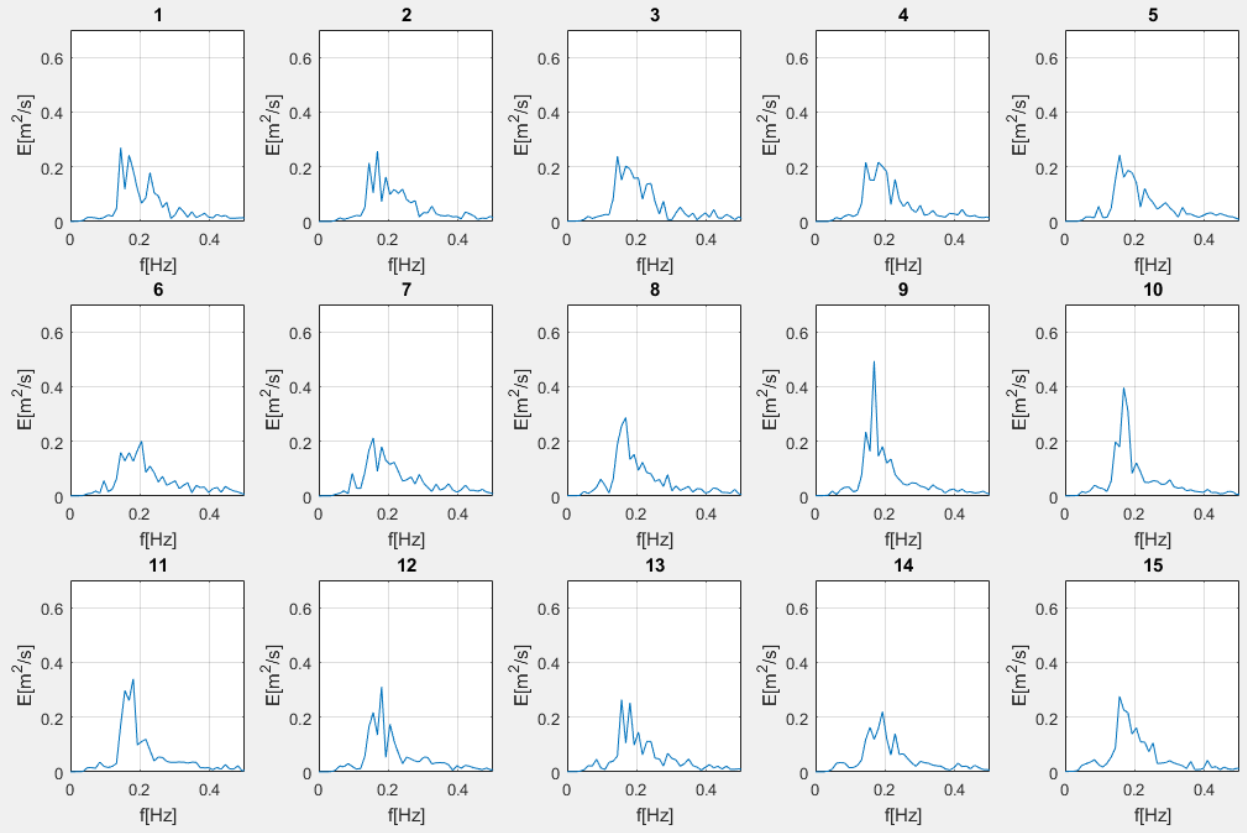

WD001_d3_s0 ebb

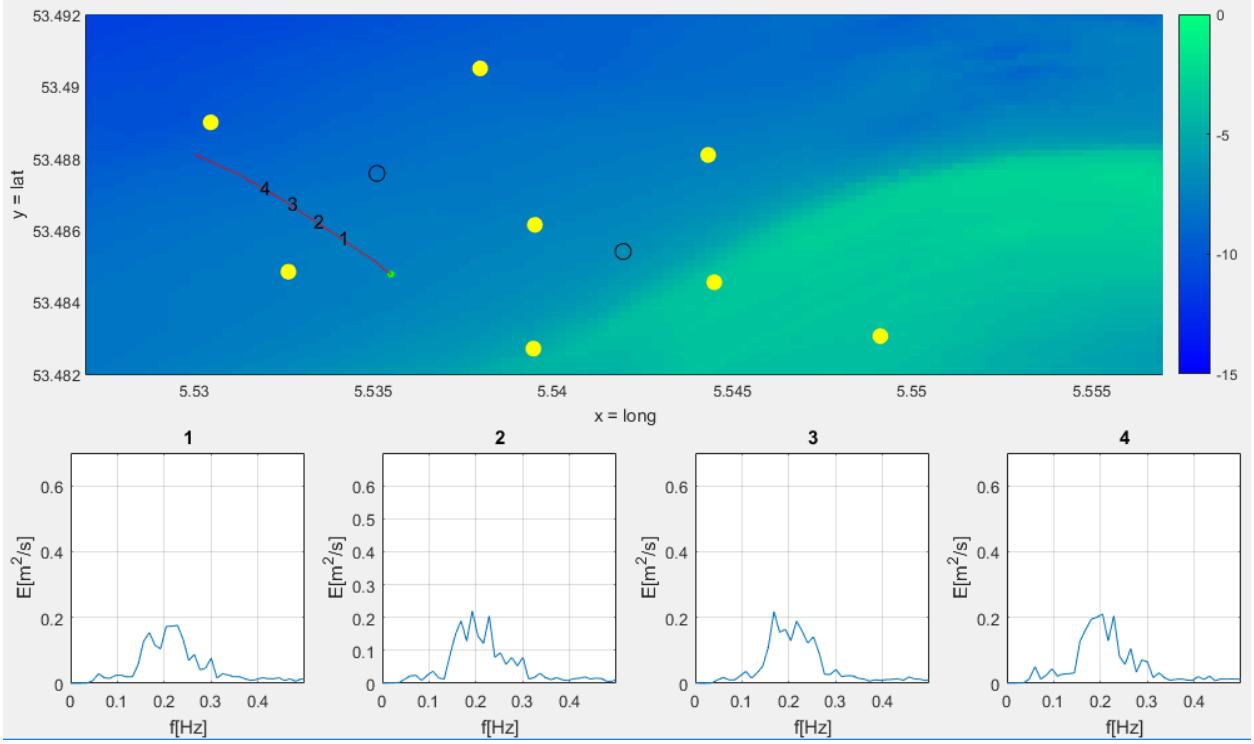

WD001_d4_s0 ebb

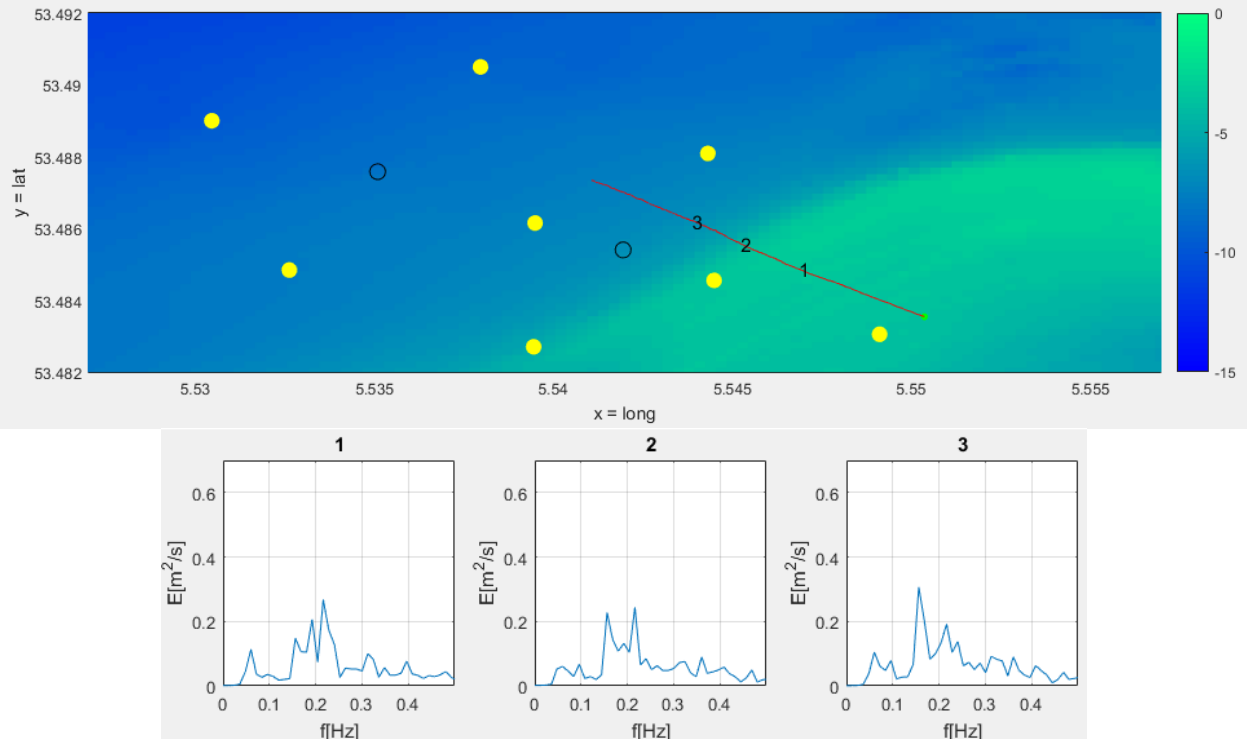

WD003_d0_so flood

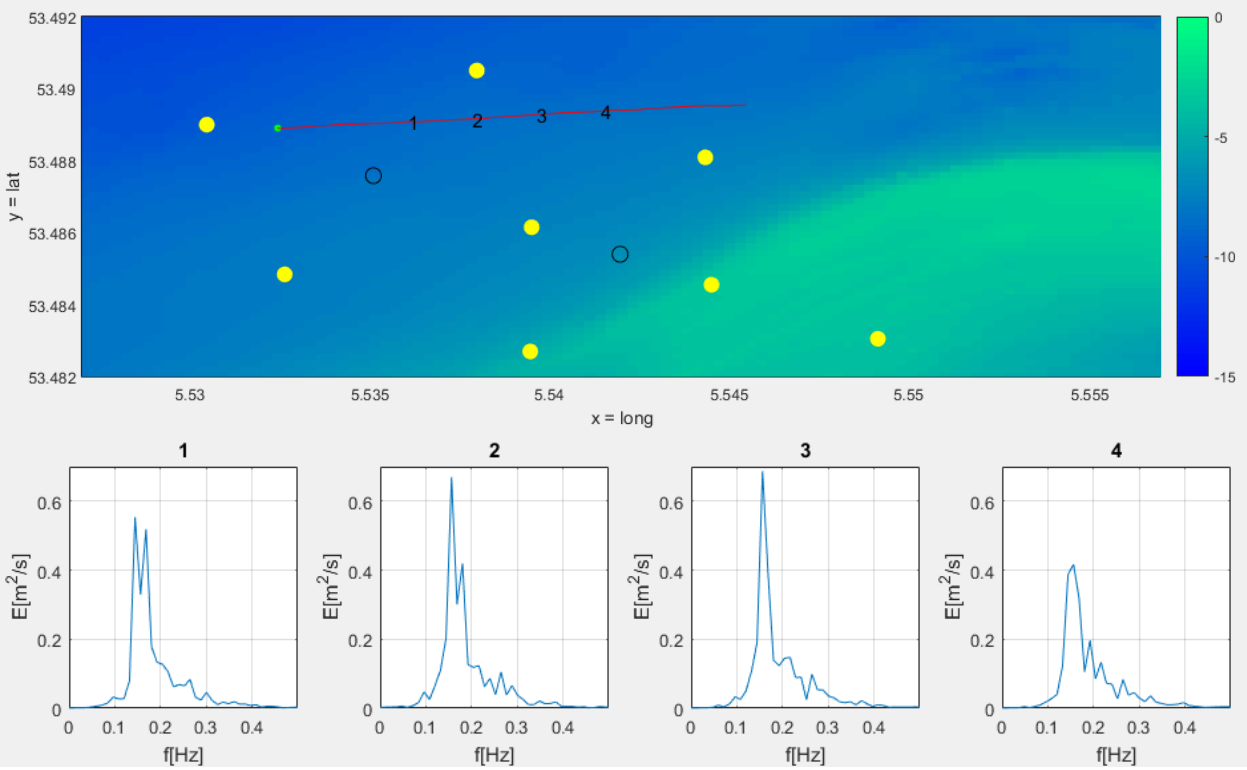

WD003_d3_so ebb